UC Berkeley
UC Berkeley Electronic Theses and Dissertations

Title

Investigation of Heterochromatin Replication Dynamics Using a Novel Method of Colocalization Analysis

Permalink

https://escholarship.org/uc/item/2ft9s8n7

ISBN

9798173786227

Author

Hickmann, Collin

Publication Date

2026-08-10

Peer reviewed|Thesis/dissertation

eScholarship.org Powered by the California Digital Library
University of California

Investigation of Heterochromatin Replication Dynamics Using a Novel Method of Colocalization Analysis

By

Collin Hickmann

A dissertation submitted in partial satisfaction of the

requirements for the degree of

Doctor of Philosophy

in

Molecular and Cell Biology

in the

Graduate Division

of the

University of California, Berkeley

Committee in charge:

Professor Gary H. Karpen, Chair
Professor Elçin Ünal
Professor Douglas E. Koshland
Professor Hernan G. Garcia

Summer 2026

Abstract

Investigation of Heterochromatin Replication Dynamics Using a Novel Method of Colocalization Analysis

by

Collin Hickmann

Doctor of Philosophy in Molecular and Cell Biology

University of California, Berkeley

Professor Gary H. Karpen, Chair

PeriCentric Heterochromatin (PCH) comprises roughly a third of the *Drosophila* genome and is organized within a compact nuclear condensate known as the PCH domain. PCH is characterized by the enrichment of methylation of histone H3 at lysine 9 (H3K9me2/3) and its reader Heterochromatin Protein 1a (HP1a), which plays a central role in the establishment of the PCH domain. Heterochromatin replication is delayed relative to euchromatin, but the mechanistic basis for this delay, its relationship to the biophysical properties of the PCH domain, and the spatial organization of PCH replication remain poorly understood.

Investigation of these questions using microscopy is frequently hampered by limitations of existing image analysis methods. The irregular morphology, high variability, and internal heterogeneity of the PCH domain make it difficult to reliably segment for object-based colocalization techniques, and its relationship with replication foci is not well described by correlation-based methods. Here, we describe FOC-Map, a new technique for the quantification and visualization of colocalization, adjacent enrichment, and exclusion. FOC-Map measures the volume-normalized overlap of segments in one channel with voxels binned by percentile intensity and distance in the other, showing how segmented replication foci are distributed across HP1a intensity bins and with varying proximity to them.

We then apply FOC-Map to time-lapse Airyscan images of cultured *Drosophila* cells and find that replication foci are enriched along the periphery of the PCH domain at the onset of late S-phase, but distributed in interspersed regions of modest HP1a intensity at later timepoints. Subsequent immunofluorescence staining for the rate-limiting replication initiation factor CDC45 reveals it to be present at reduced levels within the HP1a-rich PCH domain. We suggest a model in which exclusion of CDC45 from the HP1a-rich core of the PCH domain limits replication initiation to its periphery and contributes to its late timing. Replication-induced decondensation at the periphery

of the domain then exposes deeper layers of PCH to nucleosolic CDC45 as the interface progresses inwards until replication is complete.

Table of Contents

Acknowledgements iii

CHAPTER 1 General Introduction 1

Factors affecting heterochromatin replication timing 1

Spatial dynamics of PCH replication 3

CHAPTER 2 FOC-Map: A Novel Method for the Quantification and Visualization of Colocalization, Exclusion, and Proximity in Microscopic Images 6

Introduction 7

Results 8

Existing image analysis methods were inadequate for quantifying the organization and dynamics of PCH replication in Drosophila 8

The Fractional Overlap Coefficient: a volume-normalized colocalization metric 12

Segmentation and binning 13

Pooling across cells 16

Modularity of FOC-Map 16

Discussion 16

Interpretation of FOC-Map in Simple Control Cases 16

Interpretive complexities, peripheral enrichment, and the influence of the ROI volume 18

Alternative approaches to intensity binning and their implications for results and interpretation 19

Methods 20

Image acquisition and processing 20

FOC-Map processing and analysis 20

CHAPTER 3 Outside-in Progression of Heterochromatin Replication and Exclusion of CDC45 from the PCH Domain in *Drosophila* 22

Introduction 23

Results 24

Late-S replication foci are first enriched at the periphery of the HP1a-rich PCH domain and later in interspersed low-intensity regions 24

CDC45 foci are depleted within the PCH domain 28

Discussion 30
How CDC45 depletion in the PCH domain relates to the distribution of replication foci in early and late S-phase 32
A possible role for increasing origin firing probability in the transition to late S-phase 33
Replication-induced decondensation is consistent with internal replication patterns but insufficient to explain the initial restriction of replication to the periphery 33
Potential mechanisms underlying the depletion of CDC45 within the PCH domain, relationship to the model, and implications for other initiation factors 34
Interpretation of CDC45 foci and their relationship to replication initiation and elongation 36
The role of HP1a, outstanding questions, and future directions 37
Methods 38
Transient transfection of S2R+ Drosophila cells 38
Time-lapse image acquisition and processing 38
Live cell FOC-Map analysis 39
EdU-labelling and immunofluorescence 40
Fixed cell image acquisition and processing 40
Classification of cell cycle phase in fixed cells 41
FOC-Map analysis of fixed cells 42
Acknowledgements 42
CHAPTER 4 General discussion and future directions 43
FOC-Map as a tool for the analysis and visualization of spatial relationships in multichannel images 43
Dynamics and organization of PCH replication 43
References 46

Acknowledgements

Thank you to my advisor Gary Karpen for your mentorship, your faith in me, and your patience as I explored one rabbit-hole after another. Your enthusiasm, encouragement, and comfort with uncertainty enabled me to stick with this project through the many twists and turns along the way. I feel lucky to have had an advisor who was not only a good scientist, but a good person. Thank you to each and every member of the Karpen Lab, who have helped in countless ways big and small. Thanks to Serafin for the frequent discussions and for rapidly cloning any plasmid I could dream up without even a request. Thanks to Weiguo for the fascinating conversations. Thanks to Varsha and Lucy for helping me to organize my results and providing feedback, to Amy for mentorship and friendship during my first year, and to David for support. I'm particularly thankful for the collaboration of Gokul Upadhyayula, whose expertise in image analysis was instrumental in the development of FOC-Map. Witnessing his ability to make complex transformations of 3D images in his mind was an incredible experience, and it was a privilege to work with him. I'd also like to thank the members of my thesis committee: Hernan Garcia, Elçin Ünal, and Doug Koshland, for the guidance, the thoughtful and detailed feedback, and for helping me to simplify my aims when it was badly needed.

To my mom, dad, sister, and Brian, I truly could not have done this without your unwavering love and support. Thank you for always being there for me when I needed it. There are no words to express my appreciation. Thanks for recognizing and encouraging my curiosity from a young age and for looking the other way during my chemistry misadventures in the garage. And Dad, I'm sorry for giving you a literal heart attack a month before the filing deadline! I'm excited to have more time, energy, and mental presence to spend with all of you. Thanks to Tucker Shannon for the tungsten cube during a difficult time and for always knowing exactly what I needed to hear. Thank you to Yui Iwamoto for being a great friend, and for the Oliver Sacks book I'll now have time to read, and to Walter and Emily, for all of the memories shared. Thank you to the many other friends, family members, and colleagues not named who have enriched my life during these years and helped me to find the motivation to finish. These acknowledgements would need to be far longer than the rest of my dissertation to even come close to properly recognizing the support I have received and my gratitude for it. Thank you all.

CHAPTER 1

General Introduction

The eukaryotic genome is broadly divided into distinct organizational states known as euchromatin and heterochromatin. While the DNA in euchromatin is accessible, gene-rich, and transcriptionally active, heterochromatin is highly condensed, largely noncoding, and repressive to the transcription of most genes (Allshire & Madhani, 2018; Elgin & Reuter, 2013). Heterochromatic sequences surrounding the centromeres, or PeriCentric Heterochromatin (PCH), comprise roughly 30% of the genome in *Drosophila melanogaster* and most other metazoans (Hoskins et al., 2007). Heterochromatin is characterized epigenetically by strong enrichment for the histone post-translational modification di/trimethylation of histone H3 at lysine nine (H3K9me2/3) (Lachner et al., 2001). This modification is bound by Heterochromatin Protein 1a (HP1a), which recruits a large variety of factors involved in the maintenance and regulation of heterochromatin. The proper establishment and maintenance of heterochromatin is essential for chromosome segregation (Dernburg et al., 1996), genome stability (Wang et al., 2013), transposon silencing (Jensen et al., 1999), and the regulation of gene expression (Janssen et al., 2018).

For many years, it was thought that the compact nature of heterochromatic DNA made it sterically inaccessible to transcription (Wallrath & Elgin, 1995). However, this view struggled to explain why a subset of genes actually require a heterochromatic environment to be expressed, or how repressive compaction could also allow processes like replication and repair (Lu et al., 2000). More recently, it was revealed that weak, multivalent interactions of HP1a and other PCH components drive the clustering of heterochromatic loci into a liquid-like, membraneless nuclear body (or biocondensate) known as the PCH domain, through the process of phase separation or similar biophysical mechanisms (Larson et al., 2017; Strom et al., 2017). It has been suggested that the selective permeability and fluidity of a liquid HP1a condensate could allow more flexible control of biochemical processes at heterochromatic loci than simple compaction, but these functional implications remain unexplored (Klosin & Hyman, 2017).

DNA replication provides a particularly valuable context for examining heterochromatin accessibility, as replication machinery must reliably and directly access heterochromatic DNA within the PCH domain every cell cycle. Because complete and accurate replication of the genome is essential for chromosome segregation and genome stability, cells must ensure that even highly condensed heterochromatic sequences are replicated efficiently. This implies that either the replication machinery is permitted regulated access into the PCH domain interior, or alternatively, heterochromatic DNA may need to transiently become more accessible or relocate outside the domain for replication to occur.

Factors affecting heterochromatin replication timing

While the entire genome must be duplicated during S-phase, it does so with a characteristic temporal progression from euchromatin in early S-phase to

heterochromatin in late S-phase (Lima-de-Faria, 1959). The delayed timing of heterochromatin replication is one of its defining hallmarks, and is conserved across metazoans (Lima-De-Faria & Jaworska, 1968). Neither the mechanisms responsible for the late replication of PCH nor its functional significance are well-understood, but a growing body of evidence has ruled out some explanations while also identifying several contributing factors (Marchal et al., 2019). In early cell cycles of *Drosophila* embryos, the entire genome replicates synchronously in only a few minutes, demonstrating that late replication isn't intrinsic to heterochromatic sequences (Blumenthal et al., 1974). An early leading hypothesis was that the compact organization of PCH reduced its accessibility to both transcription and replication, leading to a delay in the replication of PCH (Priest, 1968). It has since been shown that interphase condensation of PCH precedes the onset of late replication in the early *Drosophila* embryo, indicating that PCH compaction alone cannot account for its late replication timing (Shermoen et al., 2010).

Before replication can occur, potential replication start sites, known as origins, must be loaded with the MCM2/7 helicase to achieve origin licensing (Parker et al., 2017). Licensing is limited to the G1 phase to prevent already replicated sites from being re-licensed and re-replicated in S-phase, ensuring that each part of the genome is replicated once and only once. Replication initiation occurs when several additional replication factors, including CDC45 and the GINS complex, associate with a licensed origin to form a complete replisome, allowing the origin to fire and replication to begin. Replication initiation also requires activating phosphorylation by the conserved kinases DDK and CDK2 (Costa & Diffley, 2022; Yeeles et al., 2015). Both origin licensing and initiation contribute to replication timing and are sensitive to local chromatin features, raising the possibility that the spatial organization of heterochromatin could influence timing by modulating accessibility to the factors involved in these processes or regulators of their activity (Fragkos et al., 2015).

Unlike yeast, where replication origins are defined by specific DNA sequence motifs, origins in metazoans are not strictly determined by consensus sequences, and replication initiation occurs stochastically from among many potential sites (Parker et al., 2017). Several studies have claimed that replication timing may be influenced or even explained by the distribution of licensed origins across the genome, with late replicating regions having a lower density of origins than early replicating regions (Miotto et al., 2016). Although genome-wide mapping of licensed origins has generally shown enrichment in euchromatic early-replicating regions, the methods used typically involve identifying peaks where origin licensing proteins are enriched, and these often disregard the repetitive parts of the genome that comprise much of PCH, because they cannot be uniquely mapped. This leaves open the possibility that licensing sites may be less consistently positioned in heterochromatin and therefore harder to detect as discrete peaks from population averages, even if they occur with similar frequency in individual cells. Several other methods, including SNS-seq, bubble-seq, and DNA combing identify active origins after their firing, but these techniques are unable to distinguish between differences in rates of origin licensing and firing (Hu & Stillman, 2023; Hyrien, 2015). This is because regions with high densities of active origins may reflect a higher density of licensed origins that are detected after firing, a higher frequency of origin firing among

licensed origins, or a combination of the two. One recent study estimated rates of MCM loading in *Drosophila* nuclei and observed that PCH reached similar levels of MCM loading to euchromatin by the start of S-phase, which would not be expected if late replication were the result of reduced origin licensing (Mei et al., 2022). It remains possible that the distribution of licensed origins contribute to the late replication of PCH, but the degree to which it does so remains a topic of active investigation.

In addition to origin licensing, replication timing is influenced by modulation of replication initiation. One of the best studied regulators of replication timing is RIF1 (Rap1-Interacting Factor 1; (Richards et al., 2022)). RIF1 is a conserved factor that localizes to heterochromatin and recruits Protein Phosphatase 1 (PP1) to antagonize DDK, delaying initiation until it dissociates from heterochromatin later in S-phase (Cho et al., 2022a). In the 14th round of division in *Drosophila* embryos (cycle 14), heterochromatin replication becomes delayed relative to the replication of other sequences, and this delay is driven by RIF1. RIF1's role in this process occurs prior to and independent of the recruitment of HP1a, the full heterochromatinization of PCH sequences, or their assembly into the mature PCH domains (Seller & O'Farrell, 2018). Despite this prominent early role, RIF1 plays only a minor role in the timing of PCH replication beyond cycle 14.

By the 15th round of cell division in the *Drosophila* embryo (cycle 15), one of the major PCH repeat sequences, the 359 bp repeat, is fully heterochromatinized, bound to HP1a, and part of the PCH domain. These changes are associated with a much longer delay in its replication, which persists even in the absence of RIF1. In hybrid embryos where 359 repeats are not bound by HP1a, it does not become late replicating during cycle 15, indicating that HP1a is necessary for the establishment of late replication timing (beyond the smaller delay induced by RIF1) (Yuan & O'Farrell, 2016). When HP1a is ectopically targeted to a repeat (the 1.686 satellite sequence) which ordinarily is not heterochromatinized during this developmental stage, its replication timing is delayed, similar to that of the 359 repeat. Smaller and less consistent effects on replication timing have also been noticed following the knockdown of HP1a in cell culture (Schwaiger et al., 2010). Together, these lines of evidence indicate that HP1a, and perhaps the emergent properties of the HP1a-dependent PCH condensate, play a major role in determining late replication of PCH independent of RIF1.

Spatial dynamics of PCH replication

Unlike RIF1, the mechanism by which HP1a delays heterochromatin replication remains unclear. However, HP1a is essential for organizing heterochromatin into the spatially-discrete PCH domain, and this structural role suggests a potential spatial aspect to the regulation of heterochromatin replication timing (Chen & Buonomo, 2023; Larson et al., 2017; Strom et al., 2017). While the general relationship between nuclear organization and replication timing has been widely studied, the possibility that HP1a modulates replication timing through its effects on PCH domain structure and accessibility has not been directly tested. Nevertheless, several studies have characterized where heterochromatin replication occurs relative to the PCH domain (Chagin et al., 2019; Gelléri et al., 2024; Markaki et al., 2012; Quivy et al., 2004). It has long been known that DNA replication occurs at distinct sites known as replication foci,

which can be visualized by fluorescent labelling of replisome components —most commonly the sliding clamp PCNA (Proliferating Cell Nuclear Antigen) —or nucleotide analogs introduced in pulse labelling analogs and incorporated into newly synthesized DNA (Bravo & Macdonald-Bravo, 1987; Nakamura et al., 1986). Experiments using these methods revealed a general progression of replication patterns consistent with the knowledge of replication timing. Replication foci are widely distributed throughout the nucleus in early S-phase, corresponding to the replication of euchromatin, which is loosely organized and spread throughout most of the nuclear volume. As S-phase progresses, replication is observed at a smaller number of larger and more consolidated foci before eventually converging at the PCH domain in late S-phase, at which time PCH replication occurs. While this general progression is well established, a more detailed understanding of the organization of PCH replication has only begun to develop in more recent years (Chagin et al., 2019).

Foundational work by the Almouzni group using nucleotide pulse-labeling in mouse cells observed that late-S replication foci were restricted to the periphery of PCH domains, where they formed a ring-like pattern (Quivy et al., 2004). Further pulse-chase experiments detected recently replicated DNA within the PCH domain 45 minutes after replication, even though active replication remained restricted to the periphery. This suggested heterochromatic sequences may translocate to the domain surface for replication and subsequently return to the interior after completion. This model is consistent with the understanding of the PCH domain as a region of limited accessibility, but it also offers a mechanism by which PCH sequences can be made accessible by moving out of the PCH domain. The findings also offered intriguing parallels to the translocation of heterochromatic Double Strand Breaks (DSBs) to the periphery and exterior of the domain prior to repair by homologous recombination (Chiolo et al., 2011), raising the possibility that translocation may be a more general mechanism regulating the accessibility of heterochromatin in the PCH domain.

More recent studies have challenged some aspects of this understanding while validating others. The Cremer group conducted similar experiments with nucleotide pulse-labelling in mouse cells and imaged them using super-resolution Structured Illumination Microscopy (SIM). Replication foci were observed in rings along the periphery of PCH domain in some late S-cells, but also within less compact channels within the PCH domain of others (Markaki et al., 2012; Gelléri et al., 2024). Work from the Cardoso Lab further strengthened and built upon these findings using a variety of labelling strategies in both fixed and live cells from mice and humans. They revealed a characteristic progression in which replication foci are first observed along the periphery of the PCH domain at the start of late S-Phase, then invade the interior of the domain within regions of low chromatin compaction, before finally rising to the surface again just before completion (Chagin et al., 2019). The authors proposed a model in which PCH replication begins at the surface of the PCH domain, and is later permitted or accompanied by local decondensation within the PCH domain interior, rather than larger-scale translocation of chromatin to the domain surface. It was further suggested that the earlier publications reporting a ring-like pattern of replication at the periphery of the domain may represent a snapshot at the start or end of PCH replication, but were broadly consistent with this larger progression.

Similar spatial organization has been reported in early *Drosophila* embryos, where late replication was observed primarily in decondensed chromatin adjacent to or surrounding condensed, HP1a-rich regions within the newly established PCH domain (Shermoen et al., 2010). However, more detailed, high-resolution analysis of the organization of PCH replication in *Drosophila* is lacking, and the dynamics of the accelerated cycles of the early embryo may not be broadly representative. Additionally, it remained unclear how the organization of PCH replication in *Drosophila* related to the two competing models of translocation and local decondensation developed in prior mammalian cell studies.

In this study, we set out to characterize the dynamics and organization of heterochromatin replication in cultured *Drosophila* cells, using higher resolution imaging by Airyscan microscopy and new analytic approaches to investigate these unresolved questions. This effort was complicated by several challenges: the PCH domain is irregular and lacks discrete boundaries, replication foci lie in such close proximity to the domain that blur inflates their apparent overlap, and conventional colocalization methods cannot distinguish between true overlap and peripheral enrichment without over-interpreting partial signal coincidence. To overcome these obstacles and address limitations of current analysis methods, we first developed a novel colocalization analysis technique, FOC-Map, which combines binning of one channel and segmentation of the other to enable the quantification and visualization of complex spatial relationships between irregular objects. The development and characterization of this method is reported in Chapter 2.

In Chapter 3, we successfully apply FOC-Map to elucidate the relationship between replication foci and the PCH domain through the progression of late S-phase and the duplication of PCH in *Drosophila* cultured cells. We find that replication foci at the onset of late S-phase are confined to the outer boundary of the PCH domain, forming a shell-like pattern with little overlap into the HP1a-rich interior. While similar patterns have been reported previously, our analysis confirms that replication initially occurs predominantly at the periphery of the domain rather than within the compacted interior. The early restriction of replication to the periphery prompted us to examine the nuclear distribution of the replication initiation factor CDC45, which we hypothesized might limit the capacity for initiation within the domain. As late S-phase progresses, we observe that replication begins to occur within the domain, localizing at foci within low-HP1a channels interspersed between more condensed regions. This distribution provides additional support for recent models proposing that local decondensation permits replication without the need for large-scale translocation of heterochromatic sequences to the surface of the domain (Chagin et al., 2019; Markaki et al., 2012). Finally, the broader implications of these findings and avenues for further research are discussed in Chapter 4.

CHAPTER 2

FOC-Map: A Novel Method for the Quantification and Visualization of Colocalization, Exclusion, and Proximity in Microscopic Images

Abstract

While attempting to elucidate the spatio-temporal dynamics of heterochromatin replication in live (time-lapse) and fixed samples, we observed that replication foci were associated with the periphery of the PeriCentromeric Heterochromatin (PCH) domain and with regions of low HP1a intensity. However, quantification using existing colocalization analysis methods failed to produce consistent and meaningful results. Correlation-based strategies such as the Pearson Correlation Coefficient (PCC) performed poorly due to the complex, non-monotonic relationship between signals and the large volume devoid of both signals within the nucleus. Object-based approaches such as the Manders Colocalization Coefficient (MCC) produced inconsistent results due to difficulty segmenting the nebulous, irregular, and highly variable PCH domain. Line-intensity profiles clearly displayed the preferential localization of replication foci at the periphery of the PCH domain, but were insufficiently quantitative and not amenable to analysis of larger datasets. To address these challenges, in collaboration with Dr. Srigokul Upadhyayula (UC Berkeley) we developed FOC-Map, a novel approach to quantify and visualize colocalization. FOC-Map uses an object-based approach similar to Manders, but requires only one channel to be segmented, making it well-suited for analyzing colocalization when one channel contains nebulous features with poorly-defined boundaries. FOC-Map also reveals more complex spatial associations, such as adjacency and exclusion, and gives an overview of the relationship between channels that is similar to a linescan, but is fully volumetric and more amenable to pooling in large datasets. By combining the strengths of existing methods while minimizing their limitations, FOC-Map offers a generalizable strategy for colocalization analysis that may prove useful in a wide range of imaging contexts.

Introduction

One of the most common problems encountered in cellular biology is the need to objectively quantify the spatial association or overlap between distinct features in a set of microscopic images. Despite an abundance of research into the topic, there is no gold-standard technique which is appropriate for quantifying colocalization in all images. Given the large diversity of imaging techniques used, microscopic features visualized, and types of spatial relationships measured in colocalization analysis, it is unlikely that such a generalizable strategy is even possible. All existing techniques are affected by pitfalls which limit their applicability or interpretability in certain situations, and researchers must choose the analysis method that is most appropriate for their question and dataset (Aaron et al., 2018; Bolte & Cordelières, 2006).

Existing colocalization analysis techniques can be broadly divided into three major categories: qualitative/semi-quantitative visualization methods such as line intensity profiles and intensity scattergrams, pixel correlation-based methods such as the Pearson's Correlation Coefficient (PCC), and object-based methods such as the Manders Colocalization Coefficient (MCC) (Bolte & Cordelières, 2006; Manders et al., 1992, 1993). While there is considerable overlap in how these methods may be used, they differ in their approach and in the parameters they are designed to measure (Dunn et al., 2011). The MCC measures the overlap/co-occurrence of signals: How much of the signal from one channel falls within regions occupied by the other and vice versa? This necessarily requires that the signal be differentiated from the background by segmentation, which can be challenging if the signal is not organized within well-defined structures with clear boundaries, as is often true for dynamic biocondensates.

Pixel correlation-based approaches, such as the Pearson's Correlation Coefficient (PCC), measure not just whether the signals in each channel occupy the same regions within a cell, but whether they are distributed in proportional amounts and in a linear manner. Compared to the MCC, the PCC is an indirect measure of co-occurrence. When the features in each channel extensively overlap/colocalize, high intensity in one channel will be associated with high intensity in the other, and the same will be true of low intensities. In this way, positive PCC values approaching 1 typically reflect a high degree of co-occurrence. If the features in each channel are randomly distributed with respect to one another, there will be no relationship between the intensity in each channel, and the correlation should be low or near zero. If the features tend to be mutually exclusive, high intensities in one channel are associated with low intensities in the other, and a negative correlation approaching -1 is expected (Cordelières & Bolte, 2014). This sensitivity to both co-occurrence and correlation can complicate interpretation of the results, as it can be unclear whether a difference in PCC values reflects a difference in the amount of overlap or in the proportionality of the signal. It has been argued that the PCC should only be used for images in which a linear correlation between signals can be expected, and that it can be inaccurate or misleading when applied to images with more complex relationships between channels (Dunn et al., 2011). One variant of PCC, called the Spearman's Rank Correlation Coefficient (SRC) (Adler et al., 2008), eliminates the assumption of linearity, but it still requires that the relationship between signals can be described by a monotonic function that is always increasing or always decreasing across the full range of intensities. In

images where signals are associated but not well described by linear or monotonic functions, PCC and Spearman's tend to produce ambiguous and sometimes misleading results. Despite these caveats, PCC is perhaps the most widely used quantifier of colocalization, and in practice, is often used for its sensitivity to co-occurrence by researchers who are uninterested in signal proportionality. The weaknesses of PCC are often counterbalanced by its advantages over the MCC, namely its simplicity and the fact that it does not require segmentation of the signal (Dunn et al., 2011). Given the distinct strengths and limitations of these approaches, we began by assessing the performance of several commonly used colocalization analysis methods for our specific imaging data and research questions.

Results

Existing image analysis methods were inadequate for quantifying the organization and dynamics of PCH replication in Drosophila

During our study of PeriCentric Heterochromatin (PCH) replication, we sought to characterize the spatial relationship between replication foci and the PCH domain, which is a liquid-like condensate displaying irregular and variable morphology. Specifically, we aimed to determine whether PCH replication happens within the PCH domain or is excluded from it. After collecting time-lapse images of *Drosophila* cultured cells progressing through S-Phase, we assessed whether the replication foci (labelled with PCNA) were inside the PCH domain (labelled with Heterochromatin Protein 1a or HP1a) or excluded from it at the onset of PCH replication in late S-phase. At this stage, our images displayed a qualitatively obvious relationship in which replication foci were strongly associated with the outer periphery of the PCH domain, but largely absent from its more HP1a-rich core (Fig. 1A). At later timepoints, replication foci appeared to be localized within HP1a-poor channels or voids between the more compact portions of the increasingly fragmented PCH domain (see Chapter 3 for detailed treatment).

We initially attempted to characterize this result with existing methods of colocalization analysis, but encountered several complicating factors that impeded accurate, consistent, and meaningful quantification. PCNA foci were clearly located at the outer periphery of the PCH domain, but with such close proximity that there was non-negligible overlap in the signals. If replication foci form an interface with the PCH domain, it is expected that optical blur would produce some degree of overlap, even after Airyscan Processing. Line intensity profiles (linescans) proved effective at visualizing this relationship (Fig. 1B), but they suffer from several limitations that hinder their utility in reaching a broader conclusion. First, linescans are not a volumetric method of analysis. The intensities of a single line of voxels in a single image plane are plotted, while the vast majority of information in the image is omitted. For this reason, the choice of where to draw the line can greatly influence the output. The line cannot be drawn randomly; it must pass through the center of the PCH domain and some of the PCNA foci. This makes linescans potentially prone to bias and sampling issues (Bolte & Cordelières, 2006). Furthermore, linescans are not amenable to quantitative comparison or pooling across larger datasets. Averaging together the linescans of complex features from separate cells will simply blur them together and obscure the relationship between features that may be evident in the individual linescans.

Despite these limitations, the linescan is informative for understanding why correlation-based metrics struggle with images of this type. The lefthand portion of the profile (approximately 0 to 750 nm) shows PCNA and HP1a intensity rising together above the nuclear background, as the line passes from the nucleoplasm into the region surrounding the PCH domain (Fig. 1B). This portion of the profile contributes a positive correlation between channels. At the peak of PCNA intensity, HP1a intensity dips slightly, corresponding to the peripheral localization of replication foci at regions of somewhat lower HP1a enrichment. Beyond the PCNA peak, PCNA intensity declines while HP1a intensity continues to rise as the line enters the HP1a-rich core of the domain. This portion of the profile produces a negative correlation. The relationship between channels is therefore not only non-linear but non-monotonic, violating the assumptions of both PCC, which assumes linearity, and the Spearman's Rank Correlation (SRC), which relaxes the assumption of linearity but still requires that the relationship be described by a monotonic function that is always increasing or always decreasing across the full range of intensities (Adler et al., 2008; French et al., 2008).

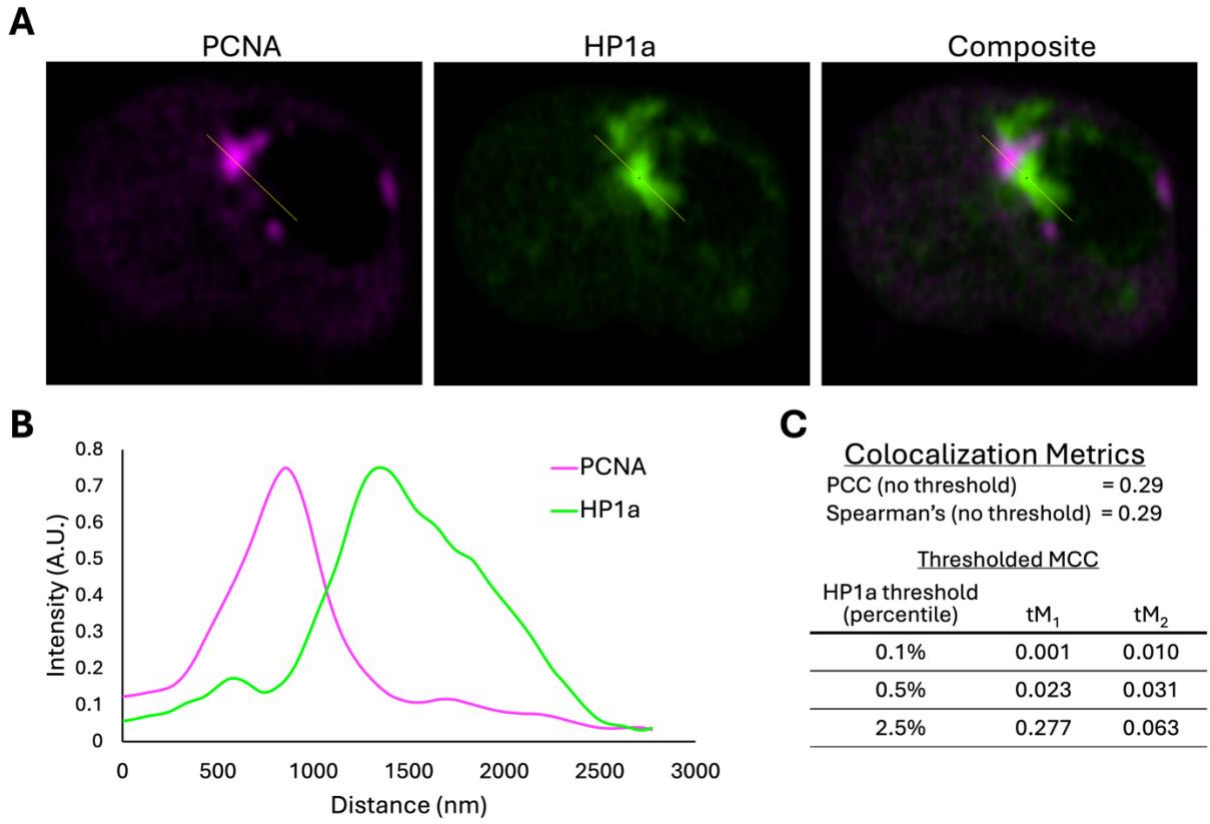


Figure 1. Commonly used colocalization metrics produce equivocal results in a cell with peripheral localization of replication foci

A. A transiently transfected S2R+ cell in late S-phase exhibits a prominent association of replication foci (mScarletI-PCNA) with the periphery of the PCH domain (mEGFP-HP1a). The yellow diagonal line passing through the brightest region in each panel is the line used for the intensity profile (linescan) plotted below. **B.** Linescans plotting the intensity of mScarletI-PCNA and mEGFP-HP1a at positions along the diagonal line in the panels above. Intensity is in arbitrary units and was rescaled using the max values to fit the plot. **C.** The values for the most commonly used quantifiers of colocalization, which were calculated from the full nuclear volume in the case of PCC and SRC, and

for the thresholded Manders Colocalization Coefficients (tM_1 and tM_2). tM_1 and tM_2 were quantified using the overlap of segmented PCNA foci and of HP1a thresholded with varying levels of stringency. The segments and their overlap are shown in Fig. 3A, which analyzed the same cell to enable direct comparison with the results of FOC-Map. The widely varying outputs show that the Manders coefficients are highly sensitive to differences in thresholding, while the intermediate values of PCC and Spearman's do not allow meaningful conclusions to be reached.

Consistent with these observations, PCC yielded a weakly positive value of 0.29 for the full nuclear volume, and SRC performed no better (Fig. 1C). The weakly positive values likely reflect the fact that both signals are elevated above the nuclear background in the same general region of the nucleus, producing a net positive correlation despite the fact that their peaks do not coincide and the signals diverge at higher HP1a intensities. These intermediate values do not permit meaningful conclusions about whether replication foci are colocalized with, excluded from, or peripherally associated with the PCH domain. Large regions of mutual exclusion or uncorrelated low intensity background are known to inflate the value of PCC, and as a result, high PCC values have previously been documented even for signals that localize in distinct organelles (Adler & Parmryd, 2010; Moser et al., 2017). All of the PCNA foci in late S-phase are located in very close proximity to the PCH domain, where HP1a signal intensity is substantially lower than in the high intensity regions of the PCH domain, but still above the nuclear background level. Thresholding can be performed to the low intensity background from the analysis, but this complicates interpretation of the result, which would then strictly measure signal proportionality rather than co-occurrence (Dunn et al., 2011). Even if PCNA foci are excluded from the high-HP1a regions of the PCH domain and preferentially located in regions of lower HP1a-intensity at the periphery of the domain, there is no reason to expect that the relationship between the signals should be inversely proportional in a linear manner. For these reasons, PCC was determined to be ill-suited for quantifying the exclusion or colocalization of replication foci with the PCH domain.

We next attempted to quantify colocalization with the thresholded MCC (tM_1 and tM_2), but encountered several distinct but closely related problems that severely limited its utility. MCC requires the boundaries of features in both channels to be defined and segmented, and works best for sharply defined features that can easily be converted to a binary mask. However, the PCH domain is nebulous and lacks clear boundaries. It contains regions of varying intensity, and there is no natural cutoff in intensity values that could be used to guide the decision. Because replication foci are located at the periphery of the PCH domain closely abutting regions of high HP1a-intensity, the way the domain is defined can dramatically affect the amount of overlap measured, making the result highly sensitive to the choice of threshold (Figs. 1C and 3A). When everything above the nuclear background level was segmented, the voids and local minima in the PCH domain were often included in it, giving the appearance of high overlap. Attempts to more stringently segment the high intensity/compact regions of the domain while excluding the voids and local minima failed to find a segmentation method that consistently accomplished this, and even if one were possible, it felt too arbitrary, prone to bias, and seemed to be a selective reporting of the results.

Interpretation of MCC values also presents challenges. It is clear in the images and the linescans that there is some overlap in signal at the periphery of the PCH domain. While MCC can determine the fraction of signal in one channel that co-occurs with features in the other, there is no clear level below which the PCH domain can be said to exclude replication foci, or above which they can be said to overlap more than would be expected in the case of adjacency. Further compounding this challenge, both the MCC and the PCC discard spatial context and obscure the nature of the association between the signals. In both the raw images and the linescans produced from them, it is evident that replication foci are located at the boundaries of the PCH domain and within local intensity minima of HP1a, but this is not reflected in either the PCC or the MCC (nor can it be).

However, the sensitivity of the Manders coefficients to changes in thresholding also suggested a potential path forward. If each threshold yields a different answer, then no single thresholded result can be considered authoritative, and selecting any one threshold risks producing an answer that is both arbitrary and potentially misleading. Yet the way in which the measured overlap varies in response to changing thresholds is not simply noise. It reflects the underlying spatial distribution of signal relative to regions of differing intensity, and may therefore contain substantially more information about the relationship between channels than the coefficient at any single cutoff. A method that systematically examines how the overlap between channels varies across the full range of intensities, rather than collapsing it into a single threshold-dependent value, could potentially extract this richer spatial information. We therefore developed the Fractional Overlap Coefficient Map (FOC-Map), which was specifically designed to retain spatial context, accommodate flexible binning strategies, and produce normalized, interpretable metrics of colocalization suitable for pooled analysis of large datasets.

FOC-Map is a modular method for quantifying and visualizing colocalization, exclusion, and spatial proximity in three-dimensional microscopy images and datasets. FOC-Map combines the volumetric robustness of correlation- and object-based methods with the spatial interpretability of linescans, while avoiding the need to select an arbitrary threshold for features with diffuse boundaries and heterogenous signal. It operates in five main stages: (1) segmentation of structures in one channel (e.g. replication foci), (2) binning of voxels in the other channel (e.g. PCH) based on intensity and proximity, (3) calculation of voxel-wise overlap within each bin, (4) normalization to account for differences in volume, and (5) visualization of the results using spatial heatmaps (Fig. 2).

Unlike traditional approaches that require both channels to be segmented, FOC-Map segments structures in only one channel (e.g., replication foci) and quantifies their distribution across percentile intensity bins in the other channel (e.g. HP1a/PCH). Quantifying the normalized overlap of the segments with each percentile intensity bin makes it possible to determine how objects in one channel are distributed with respect to regions of varying intensity in the other, while avoiding the need for a single arbitrary threshold. Voxels in the region of interest (i.e. the nucleus) are also binned by their proximity to the voxels of each intensity bin, producing a normalized distance profile that shows when segments in one channel are enriched in close proximity to high intensity regions of the other. FOC-Map is most powerful when applied to datasets containing

multiple cells, where pooling across samples reduces the influence of stochastic variability and enables more confident detection of meaningful spatial relationships.

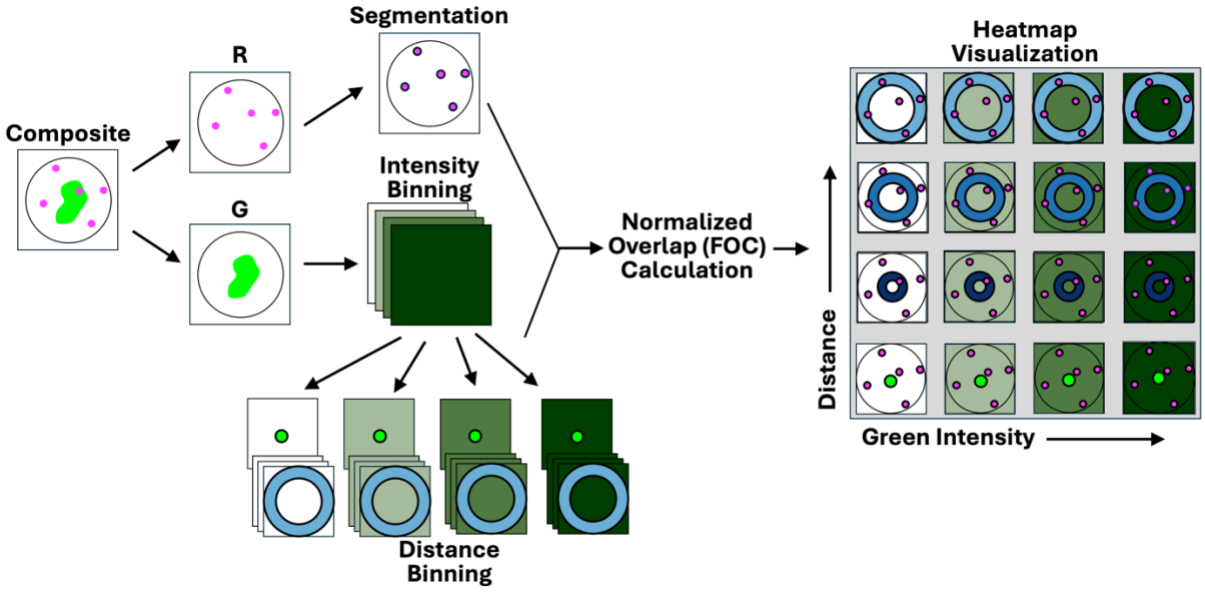


Figure 2. Overview of FOC-Map
Simplified schematic showing the workflow of FOC-Map. While features in the red channel (e.g. replication foci) are segmented, the green channel (e.g. PCH) undergoes intensity binning, and a series of distance bins is made for each intensity bin using the distance between voxels in each intensity bin of the green channel and those in segments of the red channel (Details in text and Figure 3). The FOC is used to measure the normalized overlap between the red segments and each of the green bins. These FOC values are then displayed in a heatmap. While the bin FOC values are represented graphically here, their values are conveyed by color-scaling in actual heatmaps, as shown in subsequent figures.

The Fractional Overlap Coefficient: a volume-normalized colocalization metric

At the core of FOC-Map is a normalized, object-based measure of colocalization we call the Fractional Overlap Coefficient (FOC). While conceptually similar to the MCC, the FOC introduces a normalization step that enables meaningful comparisons between bins of different sizes. This approach is particularly valuable for quantifying the distribution of objects in one channel at varying distances from high-intensity voxels in the other, as is done during distance-binning, where bin volume increases greatly with distance.

To determine how segments in one channel (e.g. replication foci) are distributed across bins in the other (e.g. HP1a intensity or distance bins), one could calculate the fraction of red segment volume that overlaps each green bin. However, when bins differ in volume, larger bins will on average harbor a proportionally larger fraction of the red segments even if the red segments are randomly distributed, preventing meaningful comparison between bins of different sizes. The MCC would be equally prone to this source of bias, as the fraction of red signal in each green bin would also be expected to scale with bin volume in the null case of random distribution.

An alternative approach might be to reverse the measurement: for each bin, calculate the fraction of its volume that overlaps the red signal. This removes dependence on bin size, but introduces a new problem: sensitivity to the total volume of red segments. If the volume of red structures doubles while their spatial distribution remains random, this fraction will increase proportionally, even though the relationship between the channels has not changed. As a result, comparisons across different cells, timepoints, or experimental conditions become ambiguous: it would be unclear whether a change in overlap reflects a change in spatial association or simply a change in signal volume. The FOC quantifies spatial association by comparing the observed overlap with that expected under a random distribution, allowing both bin and segment volume to be accounted for simultaneously. For a given bin in the green channel, the FOC is defined as:

$$FOC_{Bin} = \frac{V_{Red \cap Bin}/V_{Red}}{V_{Bin}/V_{ROI}}$$

where V_{Red}, $V_{Bin,}$ and $V_{Red \cap Bin}$ are the volumes of segments in the red channel, the bin in the green channel, and the overlap between them, respectively. V_{ROI} is the volume of the region of interest (ROI), defined as the volume in which two signals could potentially co-occur (e.g. the nucleus, for two nuclear proteins). Expressed in this way, the FOC represents the fraction of red segment volume overlapping a bin in the green channel normalized by the fraction of the total ROI volume occupied by that bin. If no spatial relationship exists between features in the two channels and their distribution is random with respect to each other, the fraction of red volume overlapping green will, on average, be equal to the fraction of the ROI overlapping green, producing an FOC of 1. An FOC of 2 would indicate the fractional overlap of the bin is twice that of the broader ROI, and twice that which would be expected in the case of random distribution. However, the FOC could just as easily be described by the inverse, as the fraction of the bin volume overlapping red segments normalized by the fraction of the ROI volume occupied by red segments. These definitions are mathematically identical. In contrast to MCC, which must be calculated separately for each channel and lacks a consistent baseline across bins, the FOC generates a single, interpretable measure that reflects both enrichment and exclusion.

Segmentation and binning

FOC-Map requires only a single channel to be segmented. The channel with the most well-defined features is typically chosen for this, allowing the channel with more complex and nebulous features to be analyzed by binning instead. While no specialized segmentation approach is required, we recommend choosing reasonably stringent parameters. Stringent segmentation reduces the risk of false-positive overlap between adjacent objects, improving measurement accuracy. However, excessively stringent segmentation may exclude genuine features, reduce segmented volumes and increase variability in measurements. A balanced approach to segmentation is therefore beneficial.

Percentile intensity binning is used to avoid the need for segmentation in the second channel. Unlike correlation-based methods, the FOC is an object-based

measure, and thus requires defined objects to quantify overlap. Traditionally, this would necessitate segmentation of both channels, which can be problematic if one channel contains diffuse or poorly defined structures. Instead, percentile intensity binning sorts voxels into groups of roughly equal size across the full intensity range, allowing the FOC to quantify normalized overlap between segmented objects and regions of differing intensity (Fig. 3a). This strategy ensures that subtle structural differences, such as those between core and boundary regions, remain discernible.

Although intensity-based binning and FOC measurements effectively quantify direct overlap between features, biological structures frequently exhibit more complex spatial relationships. For example, when two structures are adjacent or peripherally associated, some overlap at their interfaces is expected due to limitations in optical resolution. Such overlap is biologically distinct from an equal amount of overlap that is more evenly distributed throughout the entire structure, yet traditional colocalization metrics often fail to differentiate between these scenarios. To detect and quantify these more complex spatial associations, FOC-Map incorporates an additional layer of analysis called "distance binning".

While percentile intensity binning partitions voxels by their intensity values, distance binning classifies voxels based on their spatial proximity to the voxels in each of these intensity bins. Each voxel in a given intensity bin is surrounded by concentric spherical distance bins extending outward in discrete steps. All voxels in the region of interest are then grouped into these distance bins according to their radial distance from the center voxel. This process is repeated for each voxel within the intensity bin, and distance bins of equivalent radius are pooled, generating a single set of pooled distance bins containing the summed volumes and overlaps (Fig. 3b).

By quantifying overlap across these pooled distance bins, the FOC captures not only direct spatial overlap but also the enrichment of segmented features at varying distances from high intensity percentile bins (i.e. the dense regions within the features of the green channel). This approach provides key interpretative context, revealing whether overlap is evenly distributed throughout regions of high intensity or is disproportionately found in neighboring regions. Such insights significantly enhance biological interpretability, complementing direct intensity-based overlap measurements and helping to distinguish meaningful spatial relationships from artifacts introduced by imaging resolution or segmentation limitations.

Due to the multidimensional nature of FOC-Map data, conventional plots such as scatterplots or line graphs are insufficient, making heatmaps a practical necessity. Each element in the heatmap displaying the results corresponds to a specific combination of an intensity percentile bin (X-axis) and a distance bin (Y-axis), with colors encoding the corresponding FOC values. Although intensity bins are initially defined by percentile ranks, the visualization of results typically benefits from positioning these bins along the X-axis according to their average intensity. This approach addresses an important but potentially unintuitive scaling issue. For example, consider a feature that occupies roughly 10% of the diameter in a two-dimensional slice through the region of interest. Due to the cubic relationship between diameter and volume, this same feature would constitute less than 0.1% of the total three-dimensional volume. Representing all bins

with equal widths along the X-axis would cause this feature to appear disproportionately small or even visually indistinguishable on the heatmap. Scaling intensity bins by average intensity rather than strict percentile spacing preserves the visibility and proportionality of these biologically important regions, resulting in heatmaps that intuitively reflect meaningful spatial relationships within the data.

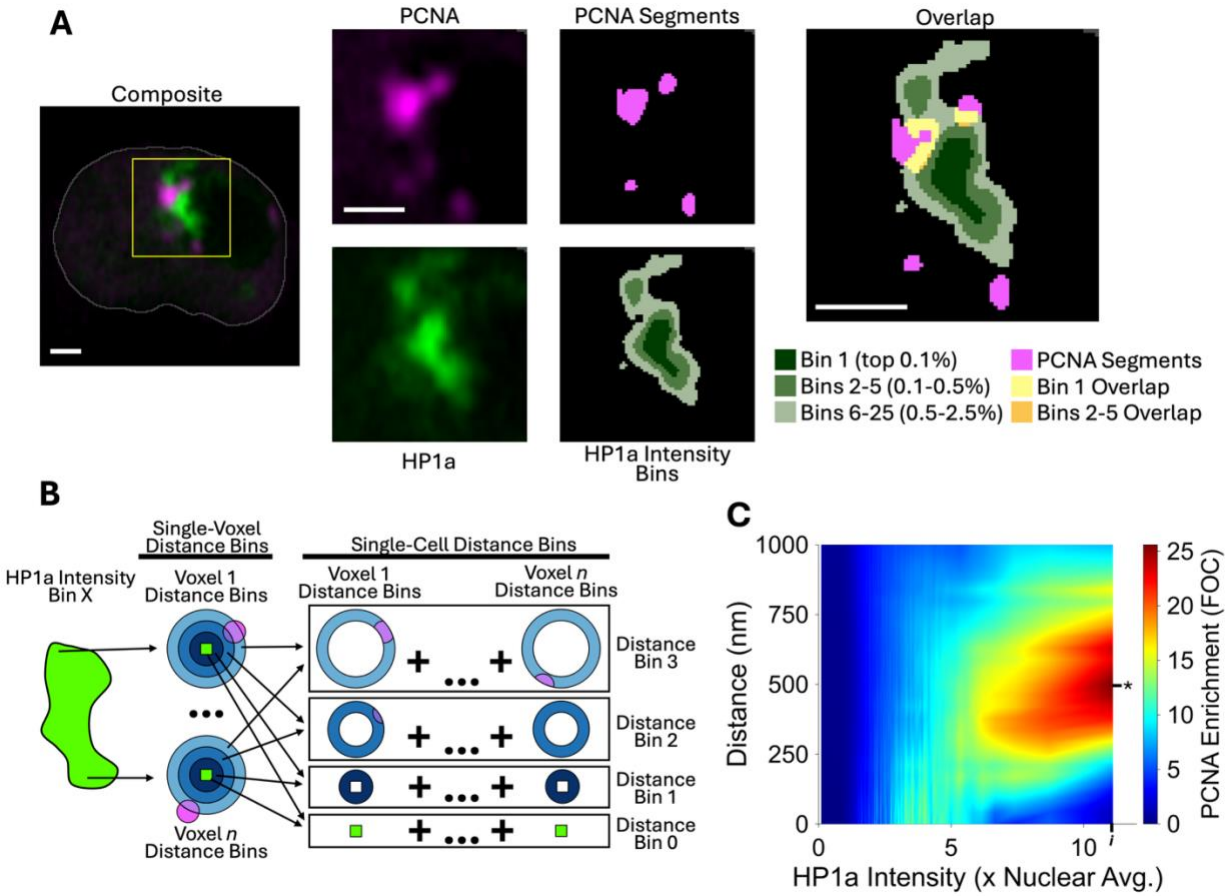


Figure 3. Visualization of FOC-Map processing steps and output in a single cell exhibiting adjacent localization between channels

A. PCNA segments and HP1a Percentile Intensity Bins visualized in a single Z-plane of a live S2R+ *Drosophila* cell in late S-Phase. PCNA (magenta) foci border the PCH domain (green, visualized with HP1a) but lack extensive overlap in the high-intensity core of the domain. Intensity bins are grouped for visibility and conceptual clarity; scale bars are 1 μm. The nucleus is outlined in grey in the first panel, while the yellow inset is magnified and displayed in all subsequent panels. **B.** Graphical representation of the distance binning procedure for a single intensity bin. Concentric distance bins are generated from each voxel within the selected intensity bin and the distance bins from each voxel are then pooled by their radii (distance from central voxel). In practice, the full set of distance bins for each voxel spans the entirety of the ROI (e.g. the nucleus) such that each voxel of the ROI is binned separately based on its distance to each voxel in the intensity bin. This process is then repeated for each intensity bin. **C.** The resulting FOC-Map for the cell shown in A. The asterisk indicates the region of peak association with PCNA segments (highest FOC value) ~500 nm away from the top intensity bin, while the "*i*" tick at the right side of the x-axis shows the highest HP1a intensity bin, where the FOC has a value of 2.5.

Pooling across cells

The procedures described above outline how FOC-Map analyzes individual cells, producing detailed profiles of spatial association for each. However, biological interpretations typically require aggregating data across multiple cells to derive general conclusions. To achieve this, FOC-Map incorporates pooling, whereby corresponding intensity and distance bins from different cells within a dataset are combined prior to calculating the FOC. Specifically, volumes of segmented objects, total bin volumes, and overlapping volumes within equivalent bins from multiple cells are summed together, and the FOC is subsequently computed from these pooled totals. This pooling strategy reduces the impact of cell-to-cell variability and provides an integrated representation of spatial associations applicable across an entire experimental condition. Although alternative approaches, such as calculating individual FOCs per cell followed by averaging, are also possible and might facilitate statistical analysis, pooling offers a straightforward method for visualizing spatial trends that may otherwise be obscured by inter-cellular noise or limited sample sizes.

Modularity of FOC-Map

FOC-Map is described here as an integrated pipeline, but its components can also be selectively implemented or combined according to the needs of specific research questions. When structures in both channels can be reliably segmented, the FOC alone can be used as a normalized alternative to the MCC, providing robust quantification of colocalization without additional binning steps. Alternatively, percentile intensity binning can be implemented without distance binning if the research question is focused specifically on direct overlap and there is no need to analyze peripheral localization or expectation for it to occur. Conversely, distance binning can be performed independently of intensity binning in cases where segmentation sufficiently defines objects of interest and intensity variations within these objects are not biologically meaningful, but assessing proximity or peripheral localization in addition to direct overlap is still desired.

However, researchers should carefully consider these simplifications, as omitting intensity or distance binning can limit the interpretative scope of the analysis and may produce misleading results. Without distance binning, FOC values above one in a particular intensity class might appear to reflect direct overlap with segmented objects. But if enrichment is substantially greater in adjacent regions than at zero distance, the apparent colocalization more likely reflects peripheral localization and optical blur at the interface rather than extensive intermixing. Similarly, omitting intensity binning may mask biologically meaningful internal variations in intensity, causing distinct subpopulations of features to be analyzed collectively, thereby diluting or misrepresenting spatial relationships that vary between regions of differing intensity.

Discussion

Interpretation of FOC-Map in Simple Control Cases

FOC-Map addresses limitations of conventional colocalization metrics by incorporating volume-based normalization and binning, making it possible to detect and

differentiate between colocalization, adjacent association, exclusion, and random distribution. However, realizing the full potential of FOC-Map requires consideration of several interpretive and methodological nuances, particularly concerning the selection of appropriate reference volumes and the implications of pooling strategies.

In its simplest application, the FOC provides a straightforward measure of spatial association, enabling direct interpretation of colocalization, exclusion, or random distribution. Control analysis on images with known colocalization or exclusion shows how the absolute FOC value reflects these relationships. In a positive control for colocalization comparing segmented PCNA foci with PCNA intensity bins (Fig. 4A), the FOC reaches a peak of over a hundred in the brightest bins (at bottom right of plot) and falls off rapidly in lower-intensity regions (at lower values on x-axis), reflecting strong colocalization as expected. In contrast, when analyzing early S-phase replication foci that are known to be euchromatic and under-represented in the PCH domain, the FOC falls well below 1 in high-HP1a bins, indicating exclusion (Fig. 4B, dark blue). These examples demonstrate how the FOC can function as a direct and interpretable readout of enrichment or depletion under appropriate experimental conditions.

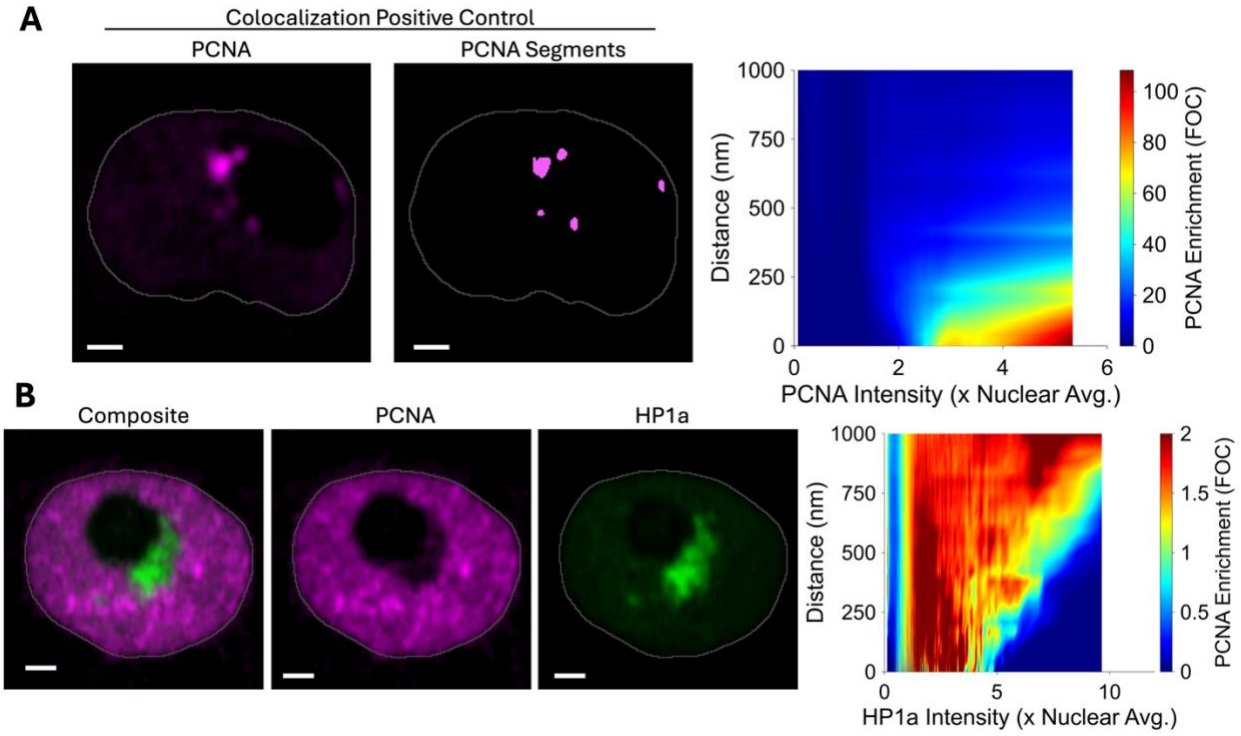


Figure 4. FOC-Map visualization of colocalization and exclusion
A. FOC-Map analysis of a positive control for colocalization visualizing the normalized overlap (FOC) between segmented PCNA foci and PCNA percentile intensity bins. **B.** A live S2R+ cell in early S-phase, when PCNA foci are enriched in euchromatic regions of the nucleus and depleted within the PCH domain. The FOC-Map showing the distribution of PCNA Foci over bins of varying HP1a intensity (x-axis) and bins of varying distance to each intensity bin (y-axis) for this cell. An FOC well below 1 indicates depletion (dark blue) in the high intensity bins (5-10x Nuc. Avg.), while the FOC above 1 reveals enrichment (orange-red) of PCNA foci in bins of low-moderate HP1a intensity (0-5x Nuc. Avg.).

Interpretive complexities, peripheral enrichment, and the influence of the ROI volume

While absolute FOC values provide clear interpretive value in cases like these, more complex spatial relationships may yield misleading results if the analysis volume does not align with the underlying biological question. This issue arises when the features being analyzed are restricted to a small subregion of the ROI, such that large volumes of mutual exclusion dominate the calculation of expected overlap. In these cases, even modest contact between features can appear as strong enrichment, not because of true colocalization, but because the null model is based on a much broader spatial distribution that the features never realistically occupy.

This problem is illustrated by the distribution of PCNA foci around the PCH domain in late S-phase (Fig. 3A). While replication foci are known to cluster tightly near the PCH domain, they are largely absent from the rest of the nucleus. Calculating the FOC across the entire nuclear volume produces values well above one even in the highest HP1a bins (Fig. 3Ci, FOC = 2.5), but this apparent enrichment reflects the improbability of any overlap under a nuclear-wide null model, rather than confirming true colocalization. In this context, the biological question is not whether PCNA overlaps HP1a more than would be expected if it were randomly distributed throughout the full volume of the nucleus, but whether that overlap occurs preferentially at the interior or periphery of the PCH domain, and whether it is concentrated in regions of high HP1a intensity near the core or in regions of lower to moderate intensity. Since the analysis volume includes large regions of the nucleus that are known a priori to be irrelevant to this question, the absolute values of the FOC are inflated and difficult to interpret.

One potential solution is to redefine the ROI more narrowly, for example by including only the region within 1-2 microns of the PCH domain. This adjustment would yield an ROI that more closely matches the null model being tested and produces FOC values with more directly interpretable magnitudes. However, this introduces new sources of subjectivity and erodes some of the key strengths of FOC-Map, such as its ability to avoid arbitrary thresholds that lack a distinct biological or physical basis. It also increases the potential for biased analysis, in which the choice of ROI is consciously or subconsciously influenced by the desired or expected result. For this reason, a more general and robust approach is to retain the full ROI but evaluate relative FOC values across bins. For example, in Fig. 3C, the FOC value for the highest HP1a intensity bin is roughly 2.5 (Fig. 3Ci), which might appear to represent meaningful colocalization if interpreted in isolation. However, when compared across bins, the FOC value of the highest bin supports a very different conclusion, as it is only 10% of the peak value located 500 nm away from the high-HP1a core of the PCH domain (Fig. 3C, asterisk). Therefore, the high-intensity HP1a regions represent a sharp local minimum in the frequency of overlap with replication foci, serving instead as the shoulder of a much larger peak corresponding to the strong enrichment of replication foci in adjacent regions of lower intensity. This relative comparison clearly shows that replication foci preferentially associate with the periphery rather than the core, underscoring how relative interpretation across bins provides clearer and more biologically meaningful insights than absolute values alone.

Alternative approaches to intensity binning and their implications for results and interpretation

Like ROI selection, the choice of binning strategy substantially impacts the quality and clarity of FOC-Map results, though it must also be tailored to accommodate variability within and between cells. Percentile intensity binning standardizes bin volumes, ensuring consistent statistical representation across cells. However, variability in the volume of biological structures between cells can result in bins that combine dissimilar voxel populations during pooling, potentially weakening or obscuring biologically meaningful patterns. In such cases, alternative binning strategies, such as intensity-range binning, may help ensure greater comparability between pooled bins. Intensity-range binning assigns voxels to bins based on predefined intensity thresholds, independent of percentile ranks. While this approach can mitigate pooling issues arising from inter-cellular differences in structural volumes, it becomes more sensitive to variability in absolute intensity levels between cells. Researchers should consider percentile binning if intensity variation is high and intensity-range binning if volume variability is more significant. Regardless of the binning approach, substantial intensity variability within individual biological structures can cause dissimilar voxels to be grouped within the same bin, diluting meaningful intensity-dependent patterns. Additional preprocessing methods such as local background subtraction or intensity normalization may help reduce these intracellular binning inconsistencies, but introduce additional complexity and must be implemented carefully to avoid unintended distortions of the underlying biological signal.

FOC-Map provides a versatile approach for analyzing spatial relationships between features in microscopy images. Its hybrid design combines the spatial interpretability of linescans with the fully volumetric analysis enabled by object- and correlation-based methods, allowing quantification of colocalization, adjacency, and exclusion within a unified framework. Because FOC-Map requires segmentation of only a single channel and incorporates percentile intensity and distance-based binning, it is especially well-suited to studies involving features with diffuse boundaries or biologically meaningful intensity variation, as well as to those examining closely abutting or spatially adjacent structures. FOC-Map offers a general strategy that is likely to be of broad utility in studies involving colocalization analysis.

Although FOC-Map already supports a diverse array of analysis strategies, its modularity permits further refinement and adaptation. Future extensions may incorporate local background subtraction or other preprocessing steps to improve the biological specificity of voxel binning within individual cells, particularly in cases of high intracellular intensity variation. In addition, alternative binning strategies could help standardize bin definitions across cells, improving consistency during pooling. Finally, statistical models may be used to estimate uncertainty or assess significance across pooled bins, enhancing the interpretability of spatial trends in aggregated datasets. As the complexity and volume of microscopy datasets continue to increase, quantitative approaches that retain spatial context while minimizing interpretive bias will become increasingly essential. FOC-Map provides a foundation for such analysis, and its continued development may help bridge the gap between qualitative image interpretation and statistically rigorous spatial quantification in cell biology. In the next

chapter, we demonstrate the utility of FOC-MAP by applying it to unresolved questions about the spatiotemporal dynamics of PCH replication.

Methods

Image acquisition and processing

The images used to demonstrate FOC-Map in this chapter are a subset of the live-cell time-lapse dataset described in Chapter 3. Full details of cell culture, transfection, time-lapse imaging, and image preprocessing, including Airyscan processing, nuclear segmentation, HP1a normalization, and PCNA foci segmentation, are provided in the Chapter 3 Methods. Briefly, cultured S2R+ *Drosophila* cells were transiently transfected with mEGFP-HP1a and mScarletI-PCNA under the control of the copia promoter (pCopia). Live cells were imaged by Airyscan confocal microscopy, with image stacks taken every 30 minutes as they progressed through S-phase. Individual nuclei were segmented from the resulting images in the HP1a channel, the extra-nuclear background was masked, and intranuclear voxels were normalized to the mean nuclear intensity. PCNA foci were segmented to produce binary masks, which were saved as a separate output file. The normalized HP1a intensity images and binary PCNA foci masks for each nucleus served as the inputs for FOC-Map analysis.

FOC-Map processing and analysis

FOC-Map processing was performed with a custom Matlab script (MathWorks R2023b). The script uses the pre-masked HP1a image input with a near-zero threshold to define the region of interest (the full nuclear volume), and all subsequent analysis steps are performed only for the voxels in this region of interest.

Within each nucleus, voxels with HP1a intensity above the nuclear background were sorted into percentile intensity bins (0.1% increments spanning the 0th to 99.9th percentile), and the average HP1a intensity of voxels in each bin was recorded. Voxel coordinates were converted from image indices to physical distances in nanometers using the voxel dimensions of the processed images (42 × 42 × 211 nm for live-cell Airyscan data) to account for anisotropic voxel geometry. Pairwise Euclidean distances were then computed between the voxels in each intensity bin and all other nuclear voxels using the MATLAB function pdist2. For each voxel in a given intensity bin, all nuclear voxels were assigned to distance bins with widths equal to the lateral voxel dimension (42 nm for this dataset). Within each distance bin, the total number of nuclear voxels and the number of PCNA foci voxels were counted. The counts from each set of distance bins were then pooled across all voxels within the intensity bin to produce a single set of distance bins for each intensity bin, as illustrated in Fig. 3B. This procedure was repeated for each percentile intensity bin. The FOC was then calculated for each combination of intensity bin and distance bin as defined in the main text.

The analyses presented in this chapter were performed on individual cells without pooling across nuclei, in order to demonstrate the method's behavior and interpretability at the single-cell level. Pooling of FOC-Map results across multiple cells within experimental conditions is described and applied in Chapter 3. For the FOC-Map shown in Fig. 4A, the PCNA foci mask was used as the segmented channel as in all other analyses, but was compared against the PCNA intensity channel rather than the

HP1a channel. This produced a FOC-Map of the distribution of segmented PCNA foci with respect to PCNA intensity bins, serving as a positive control for strong colocalization.

The binned voxel counts, average intensities, and distance bin assignments for each nucleus were stored as arrays in MATLAB .mat files. Because the FOC is derived from these stored counts, the results can be replotted with different visualization parameters, rescaled, renormalized, or pooled across cells at a later time without repeating the computationally intensive voxel-by-voxel distance and binning operations. A separate MATLAB script was used to load these stored arrays, calculate the FOC, and generate the final heatmap visualizations.

FOC-Map results were visualized as pseudocolor heatmaps with HP1a intensity on the X-axis (scaled by average bin intensity rather than percentile rank), distance on the Y-axis, and FOC encoded as color. Percentile bins left empty due to limited bit-depth in the intensity values were excluded prior to plotting. Heatmaps were rendered using interpolated shading. MATLAB scripts are available at https://github.com/collin-hickmann/FOC-Map.

CHAPTER 3

Outside-in Progression of Heterochromatin Replication and Exclusion of CDC45 from the PCH Domain in *Drosophila*

Abstract

We investigated the organization and dynamics of PCH replication in *Drosophila melanogaster*. Heterochromatin replication isn't random or uniform, but occurs in a characteristic spatial and temporal pattern. Previous mammalian studies produced conflicting models of heterochromatin replication, suggesting either that replication occurs exclusively at the periphery of the heterochromatin domain, accompanied by large-scale translocation of DNA to the domain surface, or that it also occurs internally via localized chromatin decondensation. We sought to clarify this organization in *Drosophila* cells. Using the FOC-Map analytic approach described in Chapter 2, we found that replication foci are initially concentrated at the periphery of the PCH domain at the onset of late S-phase, but later localized within low-HP1a channels throughout the domain. We then assessed the distribution of the replication initiation factor CDC45, and found that it formed nuclear puncta depleted from the PCH domain throughout the cell cycle. We propose a model in which low levels of CDC45 within the HP1a-rich PCH domain limits replication initiation to the periphery, giving rise to the shell-like pattern of replication foci that assemble at the boundary of the domain at the onset of late-S and progressively work inward until PCH replication is complete.

Introduction

Pericentric heterochromatin (PCH) is defined by enrichment for the histone modification H3K9me2/3 and its reader protein HP1a, which together maintain a condensed, largely transcriptionally repressed chromatin state. In *Drosophila* and other metazoans, these heterochromatic sequences coalesce into a membraneless biocondensate known as the PCH domain, which has been shown to form through phase separation or similar biophysical mechanisms and to exhibit condensate-like properties including selective permeability to macromolecules (Larson et al., 2017; Strom et al., 2017). Despite its compaction, PCH must be faithfully replicated every cell cycle, and it does so with a characteristic delay relative to euchromatin, a conserved feature of metazoan cell biology whose mechanistic basis remains incompletely understood. HP1a plays a central role in this delay: targeting HP1a to sequences that are not ordinarily heterochromatinized is sufficient to delay their replication, and its loss reduces the extent of late replication beyond what can be explained by other known regulators such as RIF1 (Seller & O'Farrell, 2018; Yuan & O'Farrell, 2016). How HP1a imposes this delay, whether the physical properties of the PCH domain it organizes contribute to it, and how the mechanisms responsible for the temporal dynamics of PCH replication relate to its spatial organization are open questions.

Previous studies in mammalian cells have produced two partially overlapping models describing where heterochromatin replication occurs relative to the PCH domain. Foundational work in fixed mammalian cells observed that sites of DNA replication (replication foci) during late S-phase are confined to the surface of the PCH domain, and suggested that that heterochromatic sequences may need to relocate to the domain surface in order to be replicated (Quivy et al., 2004). Subsequent studies using higher-resolution imaging found that replication foci also appeared within less compacted regions inside the domain (Markaki et al., 2012). A later study in live cells described a temporal progression in which replication begins at the periphery and later extends into the interior within locally decondensed channels, without evidence for large-scale translocation (Chagin et al., 2019). Heterochromatin replication dynamics have also been characterized in the accelerated cell cycles of early *Drosophila* embryos, where replication was observed in decondensed regions adjacent to the PCH-domain (Shermoen et al., 2010). However, it remains unclear how these findings relate to the models developed in mammalian cells and whether they hold true outside of the rapid embryonic cell cycles.

Prior efforts to characterize the spatial organization of PCH replication have relied predominantly on markers of replication elongation, such as PCNA and nucleotide analogs, to visualize sites of ongoing DNA synthesis. While informative for characterizing where replication is actively occurring, these approaches provide limited insight into the role of replication initiation in shaping these dynamics. The comparatively few studies that have addressed initiation in this context have largely focused on regulators that modulate the expression or activity of initiation factors, such as the role of RIF1 in antagonizing DDK-dependent origin activation (Cho et al., 2022b; Seller & O'Farrell, 2018). However, few have directly examined how the spatial distribution of the initiation factors themselves might influence the dynamics of PCH replication. The condensate-like properties of the PCH domain have been shown to

influence the distribution of macromolecules within it through selective enrichment and exclusion (Colmenares et al., 2025; Strom et al., 2017). Whether replication initiation factors are also affected by these properties, and whether their distribution with respect to the PCH domain influences the dynamics of heterochromatin replication, has not been directly examined. To begin addressing these questions, we focused on CDC45, a conserved component of the CMG helicase complex that is assembled at licensed origins to initiate DNA synthesis (Costa & Diffley, 2022; Ilves et al., 2010). CDC45 is present in limiting amounts relative to the MCM2-7 helicase loaded at origins, and its availability is a primary constraint on the rate of origin firing (Edwards et al., 2002; Köhler et al., 2016; Tanaka et al., 2011; Wong et al., 2011), making its distribution within the nucleus particularly likely to influence local rates of replication initiation, and by extension, the dynamics of PCH replication.

In this chapter, we set out to characterize the spatial dynamics of PCH replication in cultured *Drosophila* S2R+ cells and to investigate the distribution of CDC45 relative to the PCH domain. Using three-dimensional time-lapse Airyscan microscopy and the FOC-Map analytical approach described in Chapter 2, we tracked the progression of replication foci through late S-phase and quantified their spatial relationship to the HP1a-rich PCH domain. We found that replication foci are initially concentrated at the periphery of the PCH domain at the onset of late S-phase, forming a characteristic shell-like pattern, and that replication later extends into low-HP1a regions interspersed throughout the increasingly fragmented domain. We then assessed the distribution of CDC45 by immunofluorescence and found that CDC45 foci are depleted within the PCH domain throughout the cell cycle. Together, these results suggest a model in which the reduced availability of CDC45 and potentially other initiation factors within the HP1a-rich PCH domain limits the capacity for replication initiation in the domain interior, giving rise to the peripheral pattern of replication observed at the onset of late S-phase and contributing to the progressive, ‘outside-in’ replication of heterochromatin.

Results

Late-S replication foci are first enriched at the periphery of the HP1a-rich PCH domain and later in interspersed low-intensity regions

To determine whether heterochromatin replication occurs primarily at the periphery of the PCH domain or also in its interior, we used Airyscan microscopy to perform three-dimensional time-lapse imaging of replication foci (visualized with mScarletI-PCNA) and the PCH domain (visualized with mEGFP-HP1a) in cultured *Drosophila* S2R+ cells progressing from early through late S-phase. Consistent with prior work, cells in early S-phase exhibited numerous small, widely distributed replication foci (Fig. 1A, −20% late-S progression), reflecting widespread euchromatin replication (Bravo & Macdonald-Bravo, 1987; Nakamura et al., 1986). At the onset of late S-phase, replication foci underwent a pronounced spatial reorganization to form a distinctive shell-like pattern at the boundary of the HP1a-rich PCH domain (Fig. 1A, 20% late-S progression). As late S-phase progressed, the morphology of the PCH domain became increasingly fragmented and irregular, and replication began to occur at internal, low-intensity channels separating highly condensed HP1a-rich regions.

The pronounced changes in the morphology of the PCH domain during late S-phase made it difficult to define its boundaries consistently and objectively, limiting the effectiveness of analysis with existing colocalization methods. To determine where replication foci were localized with respect to the PCH domain without the need for arbitrary segmentation, we employed FOC-Map (described in Chapter 2). Briefly, percentile binning was used to group the voxels within each nucleus by their relative HP1a intensity, bypassing the need for segmentation of the PCH domain and making it possible to measure how PCNA foci are distributed between regions of varying HP1a intensity. To allow comparison between cells despite variation in late-S duration, we aligned the time-lapse images from each cell by their relative progression through late-S, expressed as a percentage. The HP1a-intensity bins were then pooled between the cells of each timepoint, allowing a representative result to be determined for each timepoint while minimizing the contribution of noise in single cells. PCNA enrichment is calculated for each of the pooled bins using the Fractional Overlap Coefficient (FOC), a measure of normalized overlap with PCNA foci.

In early/mid S-phase (Fig. 1B, -20% late-S progression), PCNA foci were distributed across a broad range of intensity bins with relatively low HP1a intensity, resulting in a lower peak FOC compared to later timepoints, and consistent with the dispersed replication of euchromatin during this part of S-phase. At the onset of late S-phase, replication foci became strongly enriched in bins with less than half the average HP1a intensity of the top bin. The FOC in these moderate intensity bins reached a peak of 15 (Fig. 1B, 20% late-S progression, arrow *i*), which is three times greater than the amount detected in the highest intensity bin (arrow *ii)* and 15 times greater than would be expected if replication foci were randomly distributed throughout the nucleus. This enrichment in moderate intensity bins is consistent with the preferential localization of replication foci along the periphery of the PCH domain, where HP1a intensity is lower than in the domain's core. The preferential association with lower intensity bins also holds true for later stages of late S-phase, although with lower peak FOC values that occur in bins with even lower relative HP1a intensity, consistent with the qualitative association with low intensity regions (Fig. 1B, 60 – 100% late-S progression).

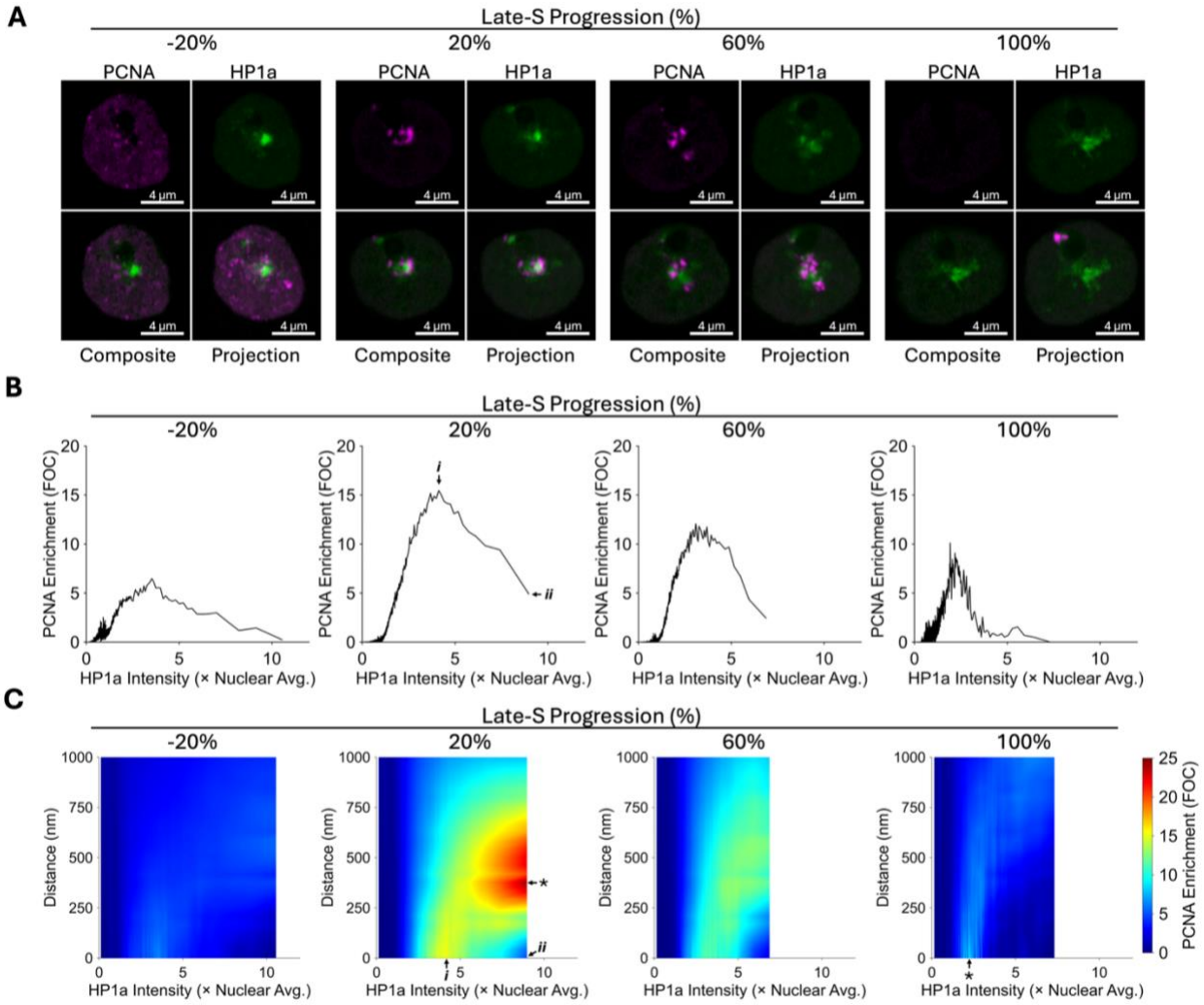


Figure 1. Late-S replication foci are enriched at the periphery of the PCH domain and in regions with relatively low levels of HP1a

A. Representative images from time-lapse analysis of cultured *Drosophila* S2R+ cells transiently expressing mScarletI-PCNA and mEGFP-HP1a, at each of the S-phase timepoints used in subsequent analysis. Replication foci form a shell at the periphery of the PCH domain at the onset of late-S, but occupy lower intensity regions interspersed between areas of greater intensity later in S-phase. Colocalization with the high-HP1a core of the PCH domain appears limited at all timepoints. Time lapses were temporally aligned by their relative progression through late S-phase, with the initial convergence of replication foci at the PCH domain defining the onset of late S-phase (0% late-S progression) and the last timepoint with replication foci defining the end of S-phase (100% progression). **B.** Pooled plots of fractional PCNA overlap vs. HP1a intensity at each timepoint (n = 10 nuclei). Nuclear voxels were binned into percentile groups with a bin size of 0.1%, the Fractional Overlap Coefficient (FOC) with PCNA was calculated for each, and the values were plotted against the average relative HP1a intensity of each bin. PCNA overlap with the high-HP1a bins increases dramatically at the 20% timepoint following the onset of late-S (arrow *ii*), but remains well below the peak overlap in much lower intensity bins (arrow *i*). **C.** Pooled FOC-Maps of fractional PCNA overlap (color) vs. HP1a percentile intensity bins (x-axis, 0.1% bin size) and binned distance from each intensity bin (y-axis, 43 nm bin size).

We next sought to quantify how fractional PCNA overlap varied with distance from high-HP1a regions. Because PCNA foci appeared to form a shell surrounding the

high intensity core of the PCH domain at the onset of late-S, we reasoned that the pattern of overlap observed in the intensity plots could be an indirect reflection of this spatial relationship. FOC-Map made it possible to visualize the spatial relationships within the images by comparing the fractional overlap of PCNA foci with the high-HP1a core of the PCH domain to that of adjacent regions. Nuclear voxels were binned by distance from the voxel with the greatest intensity of HP1a, effectively creating a series of spherical shells radiating outward from this maximum intensity voxel. This process was repeated for each of the voxels in the highest intensity bin, and the resulting distance bins from each voxel in this intensity bin were then pooled together. This was then repeated for each intensity bin. Binning was performed for all cells at each timepoint, bins were pooled between cells, and the FOC was calculated for each bin. Since binning is now being performed in two dimensions (intensity and distance), the results are plotted on a heatmap. The normalized PCNA overlap for each bin (FOC) is displayed as color. The HP1a intensity bins run along the X-axis as before, but it can now be seen how PCNA overlap varies with distance from the voxels in each intensity bin in the Y-dimension (Fig. 1C). The progression of colors from the bottom to the top of the chart at the far right displays how the FOC varies with distance from the voxels in the highest HP1a intensity bin.

The FOC-Map for the first timepoint (Fig. 1C, -20% late-S progression) shows a very broad distribution of replication foci without strong enrichment at any particular intensity class or distance, reflecting the dispersed replication of euchromatin throughout the nucleus in early/mid S-phase. In contrast, the FOC-Map for cells just after the onset of late S-phase shows a pronounced peak in FOC values 300 – 600 nm from the highest HP1a intensity bin (Fig. 1C, 20% late-S progression, asterisk), with nearly twice the FOC value of any intensity bin at zero distance. This indicates that PCNA is more highly enriched in the region adjacent to high-intensity HP1a voxels than at any particular intensity level, and reflects the “shell” configuration of PCNA foci along the boundary of the PCH domain visible in the images from this timepoint. The relationship between HP1a and distance provides further support for this conclusion. While the distance to the FOC peak for the highest intensity bin is nearly half a micron, this distance decreases with HP1a intensity in lower bins, ultimately reaching zero for the intensity bins with the highest direct overlap, which have less than half the HP1a intensity of the top bins (Fig. 1C, 20% late-S progression, arrow ***i***). The association of PCNA foci with lower intensity bins at this time may be a consequence of the fact that the HP1a-rich core of the PCH domain is surrounded by voxels with relatively lower HP1a intensity that are still well above the nuclear background. This shows that at the onset of late S-phase, replication foci directly overlap regions of low to moderate HP1a intensity bordering higher intensity regions.

At later timepoints, the enrichment of replication foci adjacent to high intensity regions decreases, and the trend in the FOC-Map is dominated by the association of replication foci with lower intensity classes rather than their proximity to high intensity regions (Fig. 1C, 100% late-S progression, asterisk). This is consistent with the observed change in the distribution of replication foci in the latter half of S-phase, where foci are primarily observed in regions of low HP1a intensity interspersed between higher intensity regions.

Rather than simply measuring the amount of overlap between replication foci and the PCH domain, FOC-Map made it possible to visualize the aggregate distribution of replication foci with respect to regions of varying HP1a intensity. This revealed that PCNA foci are most strongly enriched not within high-HP1a regions themselves, but in close proximity to them, concentrated in regions with less than half the peak HP1a intensity, at distances of 300 - 600 nm from the highest intensity voxels. This enrichment was strongest shortly after the onset of late S-phase, when the qualitative shell-like pattern was most apparent, and diminished at later timepoints as replication foci became increasingly associated with low-HP1a channels interspersed throughout the fragmenting domain. Throughout this progression, direct overlap with the HP1a-rich core remained consistently low relative to the enrichment observed in adjacent and lower-intensity regions. These patterns are broadly consistent with qualitative observations made here and in prior work, but the quantitative detail provided by FOC-Map goes beyond what could be determined by visual inspection alone. In particular, the ability to distinguish peripheral enrichment from direct overlap and to track how this relationship changes with both intensity and distance reveals spatial structure in the data that would otherwise be obscured. The near-absence of replication foci from the domain interior at the onset of late S-phase raises the question of what constrains replication to the periphery during this initial phase, and how this pattern might relate to events upstream of the replication elongation visualized as replication foci.

CDC45 foci are depleted within the PCH domain

We reasoned that the observed restriction of replication to the surface of the PCH domain at the onset of late S-phase could result from decreased replication initiation in its interior. While there is no established method for the visualization of initiation sites *in situ*, the initiation factor CDC45 is known to be rate limiting for replication initiation, and its distribution within the nucleus would therefore be expected to influence local rates of initiation. Motivated by the past work showing that the PCH domain may partially exclude some factors by selective permeability (Strom et al., 2017), we hypothesized that CDC45 is excluded from the PCH domain. To test this hypothesis, the distribution of CDC45 and its relationship to the PCH domain was characterized by immunofluorescence staining in fixed S2R+ *Drosophila* cells. Immunofluorescence allowed endogenous CDC45 to be visualized without the artefacts that are known to occur with its ectopic expression in live cells (Köhler et al., 2016). Cell cycle stage was determined using a combination of EdU-labelled replication foci and DNA content (integrated nuclear DAPI), allowing cells in G1 phase, early S-phase, late S-phase, and G2 phase to be differentiated from each other.

Staining for CDC45 revealed a punctate nuclear distribution in all stages of the cell cycle, but with highly variable intensity between cells (Fig. 2A). Although prior studies have shown that CDC45 remains associated with the replisome during elongation (Aparicio et al., 1997), CDC45 puncta were distinct from replication foci visualized by EdU labelling (Fig. 2A), with minimal apparent overlap between the two signals. It is unclear whether the apparent lack of visible CDC45 enrichment at elongating replication foci indicates that only a small fraction of CDC45 is associated with elongating replication forks at any given time in S-phase, or instead suggests that

our antibody has difficulty accessing or recognizing the epitope in elongation-associated CDC45. Since the current aim is focused solely on CDC45's role in replication initiation, the negligible level of signal from elongation-associated CDC45 simplifies the quantitation and interpretation of the results.

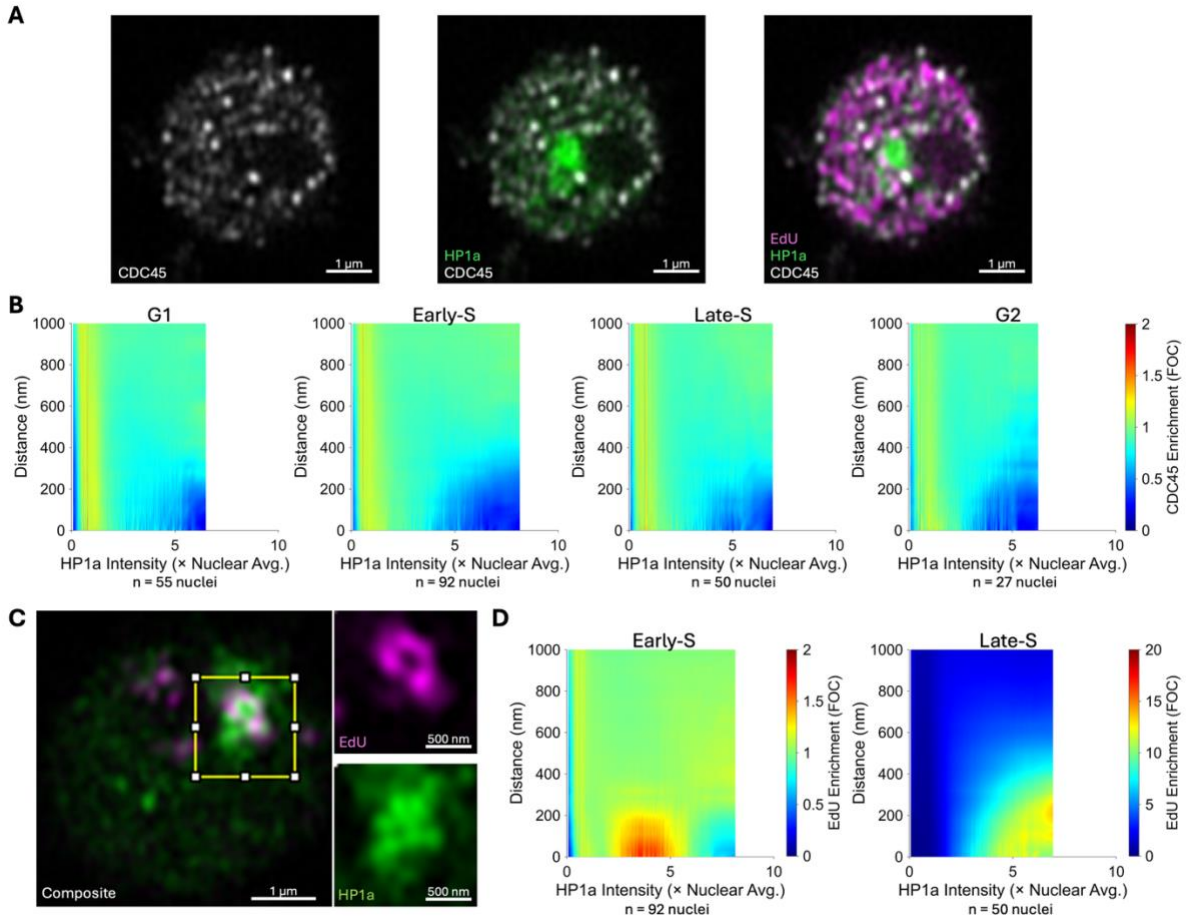


Figure 2. CDC45 foci are excluded from the PCH domain

A. Representative immunofluorescence image of a fixed S2R+ cell in early S-phase stained for HP1a (green) and CDC45 (gray) after pulse-labelling with EdU to mark replication foci (magenta). CDC45 forms nuclear foci that seem to be present at reduced levels within the PCH domain relative to the rest of the nucleus. **B.** Pooled FOC-Map of Fractional CDC45 overlap with nuclear voxels binned by percentile HP1a intensity (X-axis, 0.05% bin size) and distance from each intensity bin (Y-axis, 35.5 nm bin size). During all phases of the cell cycles, overlap of CDC45 foci with high HP1a-intensity bins is strongly reduced below the nuclear average of 1.0. **C.** Representative image of EdU foci and HP1a in late S-Phase. EdU foci appear to form a shell around high-HP1a regions that is qualitatively similar to PCNA in live cells, but the reduced scale of the structures in fixed cells approaches the resolution limit and increases the apparent overlap. **D.** Pooled FOC-Maps displaying the normalized overlap (FOC) of EdU foci with nuclear voxels binned by percentile HP1a intensity (X-axis, 0.05% bin size) and distance from each intensity bin (Y-axis, 35.5 nm bin size) in the same cells quantified in Fig. 2B.

Segmentation of CDC45 foci allowed colocalization with HP1a to be measured by the same FOC-Map approach used for PCNA, while also reducing the contribution of low intensity background and autofluorescence. Quantitation revealed that fractional overlap of CDC45 with high-HP1a regions is extremely low. The FOC of the highest HP1a intensity bin was under 0.2 in both early and late S-phase, indicating that the level

of overlap with these regions was less than one fifth of the average throughout the nucleus. Similar depletion was also observed during G1 and G2 phase, suggesting that the scarcity of CDC45 foci within the PCH domain isn't simply a consequence of CDC45 sequestration at euchromatic initiation sites in early S-phase.

Notably, the HP1a-rich PCH domain has far less overlap with CDC45 foci than was measured with PCNA foci in live cells (compare Fig. 2B and Fig. 1C). While the FOC value for PCNA foci in high HP1a intensity bins is only a fraction of the peak FOC in lower intensity bins and neighboring regions, it does not consistently exhibit true depletion below the nuclear average, as would be indicated by FOC values of less than one. This is in contrast to the broad depletion of CDC45 in high HP1a bins observed at all stages of the cell cycle. While EdU labelling was primarily used to discern cell-cycle stage, it also offers an orthogonal approach to visualize elongation sites and their relationship to the PCH domain. More importantly, the amount of HP1a-overlap with CDC45 foci and replication foci (EdU) can be compared in the same cells. As expected, EdU foci had a similar distribution and morphology to PCNA foci observed in live cells, and their relationship with the PCH domain appeared qualitatively similar. Many cells in late-S phase appeared to have a "shell" of EdU foci surrounding the PCH domain, similar to what was observed for PCNA at the onset of late S-phase in live cells, while others had a morphology resembling those in the latter half of late-S, with EdU foci interspersed in channels of relatively low HP1a intensity sandwiched between higher intensity regions (Fig. 2C). EdU foci exhibited more overlap and closer proximity to high-intensity regions than was observed in live cells (Fig. 2D), but this is likely an artefact of decreased effective resolution due to cell shrinkage during fixation or processing. CDC45 colocalization with the PCH domain was likely also affected by the shrinking, but this would be expected to bias the result towards greater colocalization with the domain. The relatively strong depletion of CDC45 foci within the PCH domain detected despite this issue strengthens the result, especially when it is compared to that observed for both EdU and PCNA. We conclude that CDC45 foci are present at reduced levels within the PCH domain throughout the cell cycle, and suggest that this may contribute to the replication dynamics observed in live cells.

Discussion

Our results reveal that heterochromatin replication proceeds in an outside-in progression, beginning at the periphery of the PCH domain at the onset of late S-phase and later extending into low-HP1a regions interspersed throughout its interior, consistent with the progression reported in recent mammalian studies (Chagin et al., 2019; Gelléri et al., 2024; Markaki et al., 2012). Combined with the observed depletion of CDC45 foci within the PCH domain, these results support a model in which reduced levels of CDC45 in the PCH domain limit the frequency of replication initiation in its interior. This model would help to explain multiple aspects of heterochromatin replication dynamics. First, it would explain the characteristic shell pattern that is observed at the onset of late S-Phase. If the exclusion of CDC45 suppresses initiation inside the PCH domain, initiation of heterochromatin replication would be expected to preferentially occur at the periphery of the domain, which forms an interface with the nucleosol. As replication forks move inward or pull heterochromatin out, more heterochromatin would

be made accessible at the advancing interface, and this process would continue until replication is complete, consistent with the observations made here and in previous work (Chagin et al., 2019; Quivy et al., 2004). Second, this model could help to explain the temporal dynamics of heterochromatin replication. If replication initiation were limited to the interface of the PCH domain, only a small fraction of heterochromatin would be accessible for replication at any given time, which would be expected to delay its overall timing. While this study focused on CDC45, it is possible that other initiation factors are similarly depleted within the PCH domain, and this would be expected to strengthen the impact on replication dynamics.

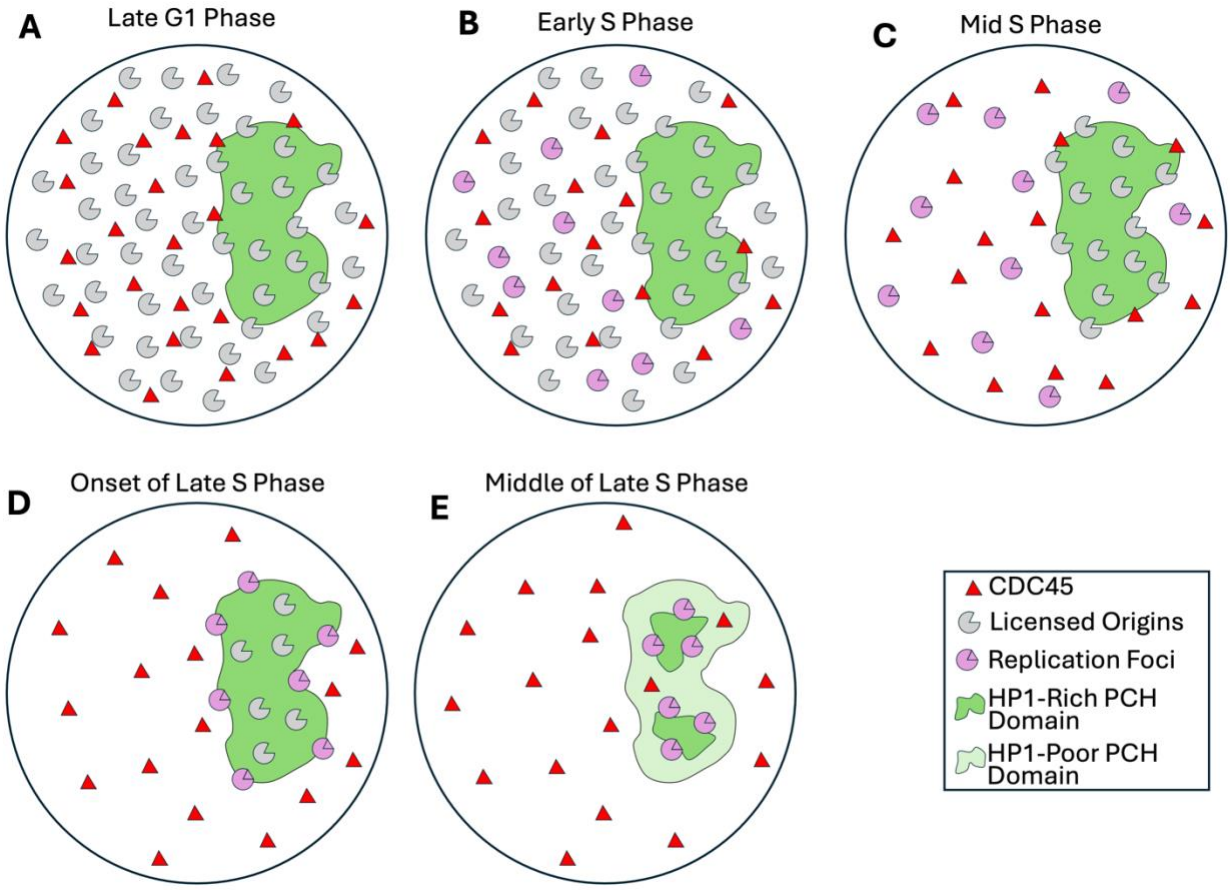


Figure 3. A Model for the influence of CDC45 distribution on PCH replication dynamics

A. CDC45 foci are depleted within the PCH domain throughout the cell cycle. Licensed origins are present in excess to CDC45 throughout the nucleus, causing CDC45 to be the limiting factor for replication initiation. **B.** At the start of S-phase, the higher concentration of CDC45 foci outside the PCH domain causes euchromatic origins to fire at a higher rate than those inside the PCH domain. **C.** By mid-S Phase, the concentration of licensed origins decreases as most of the chromatin outside the PCH domain is replicated, and origin concentration becomes the limiting factor. **D.** As decreasing origin concentration limits the rate of replication initiation outside the PCH-domain, the greater concentration of origins at the interface between the PCH domain and the nucleosol leads to a higher relative rate of replication initiation there. This creates the “shell” of replication foci and marks the start of late-S and heterochromatin replication. CDC45 remains depleted within the PCH-domain, so replication is primarily

initiated at the outer periphery. **E.** Replicated PCH at the periphery of the domain temporarily decondenses and/or dissociates from HP1a, allowing CDC45 to initiate replication at the newly exposed interface between deeper layers of unreplicated HP1a-rich PCH and the HP1a-poor regions where replication is already underway.

How CDC45 depletion in the PCH domain relates to the distribution of replication foci in early and late S-phase

In late G1 and at the start of S-phase, origins licensed with the MCM2-7 helicase complex greatly outnumber the initiation factor CDC45 (Fig. 3A-B). Only a small minority of these origins initiate replication over the entirety of S-phase, with an even smaller fraction active at any given point (Ibarra et al., 2008; Powell et al., 2015). Licensed origins compete for the recruitment of CDC45, which was previously shown to be rate-limiting for replication initiation in species ranging from budding yeast to mammals (Edwards et al., 2002; Köhler et al., 2016; Tanaka et al., 2011; Wong et al., 2011). The observed depletion of CDC45 within the PCH domain is therefore likely to have a disproportionately large influence on the rate of replication initiation, resulting in a reduced frequency of initiation events within the domain relative to the euchromatic regions outside it. This difference in initiation rates provides a simple explanation for the early-S pattern of replication foci, in which replication is predominantly observed throughout euchromatic regions and largely excluded from the interior of the PCH domain.

While this relationship is fairly straightforward in early S-phase, where the distribution of CDC45 is broadly similar to the distribution of replication foci, it grows more complex at the onset of late S-phase. This transition is characterized not only by a decrease in euchromatin replication, but by an increase in heterochromatin replication at the surface of the PCH domain, yet no corresponding increase in CDC45 is observed at this location. We propose that this apparent contradiction can be resolved if two effects are taken into consideration. First, as an increasingly high fraction of the euchromatin distributed throughout the nucleus is replicated during early S-phase, there is a decrease in the remaining number of licensed origins that may associate with CDC45 to initiate replication, while CDC45 is released from disassembled CMG complexes at terminated replication forks and made available for initiation at new sites (Fan et al., 2021). Eventually, the declining number of licensed origins becomes the limiting factor for replication initiation outside of the PCH-domain. As a consequence, fewer new replication foci would form in these regions, and an increasing proportion of replication foci would be found at the domain's surface where licensed origins remain in excess (Fig. 3C). While this effect may explain the change in the distribution of replication foci in relative terms, it is inadequate to account for the absolute increase in the amount of replication occurring at the periphery of the PCH domain at the onset of late S-phase, underlying the need for another mechanism that might be responsible for the kinetics of this this transition.

A possible role for increasing origin firing probability in the transition to late S-phase

Past efforts to model the relationship between origin licensing, activation, and replication timing addressed a similar discrepancy by suggesting that origin firing probability increases with the progression of S-phase, keeping the overall rate of replication from declining prematurely as the number of unreplicated origins decreases (Goldar et al., 2009; Rhind et al., 2010). When combined with the relative increase in the fraction of initiation events occurring at the surface of the PCH domain, this effect may explain the increased abundance of replication foci observed at this region during the transition to late S-phase. The tight coordination between the decrease in euchromatin replication and increase in PCH-associated replication foci may be particularly well-explained by a negative feedback loop that globally regulates replication initiation rates.

One intriguing candidate for such a role is the ATR-Chk1 pathway. While ATR-Chk1 is well-known for its activation of the intra-S checkpoint in response to replication stress, it is also activated at lower levels by DNA replication in unperturbed cells, where it limits excessive origin firing in early S-phase (Ciardo et al., 2019; Menolfi et al., 2023; Moiseeva et al., 2019). As licensed origins outside of the PCH domain grow sparse in mid S-phase and the rate of new initiation events begins to decline, there may be a corresponding decrease in activation of ATR-Chk1 and a relaxation of its antagonism of further origin firing, increasing the firing probability for the remaining origins. This would be expected to accelerate the completion of euchromatin replication outside the PCH domain and to further promote the relaxation of inhibition by ATR-Chk1. The further relaxation of inhibition from ATR-Chk1 would then cause an increase in the rate of origin activation at the remaining CDC45-exposed origins, which are located at the interface between the PCH domain and the rest of the nucleus. Together, these effects would produce the abrupt transition to late S-phase and the shell-like pattern of replication foci surrounding the PCH domain observed at this time. Supporting this hypothesis, prior studies have shown that cells in early S-phase are more sensitive to the effects of ATR inhibition than those in late S-phase, and that ATR-Chk1 suppresses CDK1-mediated origin firing in early S-phase but not in late S-phase (Katsuno et al., 2009; Menolfi et al., 2023).

Replication-induced decondensation is consistent with internal replication patterns but insufficient to explain the initial restriction of replication to the periphery

Two distinct patterns of replication were observed during late S-phase. While replication was initially limited to the periphery of the PCH domain at the start of late S-phase, it was later observed in regions with relatively low HP1a levels interspersed between regions of higher intensity. The low HP1a intensity in these regions may reflect localized heterochromatin decondensation induced by ongoing or recent replication, partial dissociation of HP1a, or a combination of the two. While the methods used here cannot directly distinguish between these possibilities, our results closely match the pattern of locally decondensed replication sites observed within the PCH-domain in prior works, and the broader model is compatible with both potential mechanisms (Chagin et al., 2019; Gelléri et al., 2024; Markaki et al., 2012).

Because decondensation is a known consequence of replication, it may initially seem to challenge the need for an additional mechanism to explain the relative scarcity of replication within the highly compact, HP1a-rich core of the PCH domain. Any replication occurring within these compact regions would necessarily induce local decondensation and reduce HP1a intensity, creating an apparent exclusion of replication foci from regions of high HP1a intensity. However, this is not sufficient to explain the observed distribution of foci at the start of late S-phase, when they are associated with the domain's surface rather than decondensed regions within it. If replication initiation occurred randomly in heterochromatin and were not influenced by the organization of the PCH domain, replication foci should initially appear with comparable frequency throughout the domain, each coinciding with localized regions of low HP1a intensity caused by ongoing replication. Instead, replication foci were observed predominantly at the periphery of the domain at the onset of late S-phase, producing the characteristic shell-like pattern described above. Only later in the progression of late S-phase did replication foci appear deeper within the PCH domain at interspersed, locally decondensed regions. This sequential pattern strongly suggests that replication-induced decondensation, while influencing local chromatin structure, cannot itself explain the peripheral localization of replication foci observed at the start of late S-phase. The distribution of CDC45 offers an explanation for these dynamics, as described in the above proposed model.

Potential mechanisms underlying the depletion of CDC45 within the PCH domain, relationship to the model, and implications for other initiation factors

While the experiments conducted are unable to determine why CDC45 is present at reduced amounts within the PCH domain, the results are consistent with the partial exclusion of CDC45. Such an effect may be mediated by the domain's condensate properties, which have previously been shown to produce selective permeability and partially exclude inert macromolecular probes (Strom et al., 2017). It could also be the result of affinity partitioning, in which a lack of favorable interactions with other components of the PCH domain or presence of favorable interactions with nucleoplasmic components would be expected to concentrate CDC45 in the nucleoplasm and deplete it within the PCH domain (Larson & Narlikar, 2018; Walter & Brooks, 1995). If CDC45's exclusion from the PCH domain is mediated by its condensate properties, then replication-induced decondensation and dissociation of HP1a at the domain's periphery would be expected to render these regions accessible to CDC45, exposing a new interface of unreplicated, condensed PCH. In this way, initiation would remain limited to the interface between condensed and decondensed regions, but successive rounds of replication and decondensation would progressively advance this interface inward, consistent with the outside-in progression observed in the time-lapse data.

Although the CDC45 FOC-Maps do not show an obvious increase in CDC45 overlap with the PCH domain during late S-phase, this is not necessarily inconsistent with the model. CDC45 is not specifically enriched at sites of replication in the way that PCNA and EdU are; rather, it is expected to be present at roughly nucleoplasmic levels in any region not sufficiently condensed to exclude it. Regions that have decondensed

during replication would fall into low-HP1a intensity bins rather than high-HP1a bins, so CDC45 in these regions would not register as overlap with the condensed domain interior on FOC-Map. This contrasts with EdU and PCNA, which are specifically concentrated at replication foci and therefore produce strong, localized enrichment that is detectable even when resolution limitations spread some of their signal into higher-intensity bins. Additionally, the fixed-cell data pools all late-S cells together regardless of their progression through the inward replication sequence, so any increase in CDC45 access to newly decondensed regions at later stages would be diluted by cells at earlier stages where the shell pattern predominates.

The results also argue against several alternative potential explanations. Unlike PCNA, CDC45 was not observed to form foci colocalizing with sites of active replication, so its relative scarcity in high-HP1a regions of the PCH domain cannot be expected to occur solely as a consequence of replication-induced decondensation during S-phase. Another possibility is that CDC45's localization within the nucleus might reflect its recruitment to licensed origins. If this were the case, its uneven distribution might be caused not by exclusion from the PCH domain, but by reduced recruitment to origins inside the domain or preferential recruitment to origins elsewhere. This could occur for multiple reasons. Heterochromatin-associated factors could directly or indirectly inhibit the recruitment of CDC45. For example, RIF1 is known to be enriched in the PCH domain and inhibit origin activation by antagonizing DDK activity (Cho et al., 2022b). Because DDK activity is required for CDC45 recruitment, RIF1 could also suppress CDC45 loading, although this has not yet been directly tested. Alternatively, if licensed origins are sparser in heterochromatin than in euchromatin—as has been suggested by some results but contested in others (MacAlpine et al., 2010; Mei et al., 2022; Miotto et al., 2016; Powell et al., 2015)—this could also reduce CDC45 recruitment in the PCH domain.

However, these mechanisms are less consistent with our results for multiple reasons. First, if CDC45’s localization directly reflected its recruitment to or association with licensed origins, its localization should shift to the PCH domain during heterochromatin replication in late S-phase, after the exhaustion of euchromatic origins outside of the PCH domain—yet no such shift was observed. Second, CDC45's exclusion from the PCH domain was also observed in G1 cells that lacked origin activation or replication and in G2 cells with no licensed origins at all. Therefore, while differences in origin licensing and activation may contribute to replication dynamics and timing, they cannot explain the reduced levels of CDC45 within the PCH domain and their persistence throughout the cell cycle.

If selective permeability, affinity partitioning, or a similar mechanism is responsible for CDC45’s partial exclusion from the PCH domain, it’s possible and perhaps likely that other factors required for replication initiation are also affected by these mechanisms and distributed in a similar manner. If multiple initiation factors are partially excluded from the PCH domain, this would be expected to produce a synergistic effect on the rate of assembly of the mature CMG complex and consequent origin firing. This could help to explain how the partial exclusion of CDC45 would result in a near total absence of replication foci within the PCH domain until the final stage of late S-phase, following extensive replication and decondensation at the domain's

periphery. If licensed origins are more frequent in euchromatin than heterochromatin, this might also contribute to the observed dynamics in a similar fashion, although the stoichiometric excess of licensed origins makes it likely that its influence on replication timing would be lesser than that of CDC45 and other initiation factors.

Interpretation of CDC45 foci and their relationship to replication initiation and elongation

The nuclear localization of CDC45 is in broad agreement with past results that have visualized the protein, but its distribution within the nucleus has been more variable between studies with differing cell types and visualization techniques. Some studies observed colocalization with sites of ongoing replication, as might be expected based upon CDC45's membership in the replicative CMG complex, but the studies reporting this localization did so only after removal of the soluble protein fraction prior to fixation, within the atypical context of Chorion amplification, or after potentially disruptive synchronization with thymidine blocks (Bauerschmidt et al., 2007; Loebel et al., 2000; Polasek-Sedlackova et al., 2022). Other studies are in better agreement with the localization observed in the present work, finding broad nuclear localization with diffuse or punctate distribution that does not colocalize with replication foci (Broderick, 2012; Köhler et al., 2016; Wong et al., 2011). The pan-nuclear distribution seems to be more common when CDC45 is visualized without removal of the soluble protein fraction, as is the case in the present study. A lack of visible association with replication foci despite an essential biochemical role in replication would not be unique to CDC45, as it has been well documented for other replication proteins, most notably in the case of the MCM complex (Dimitrova et al., 1999; Marinsek, 2010; Wong et al., 2011). This paradoxical lack of colocalization may be caused by epitope masking within the fully assembled CMG complex, although this explanation is made less likely in the present study by prior validation of the antibody used here through immunoprecipitation of the full CMG complex (Moyer et al., 2006; Polasek-Sedlackova et al., 2022). It might also result from a large fraction of CDC45 that is soluble, bound to origins that have not yet fired, or associated with other structures, in which case the signal from these other populations might drown out the signal that is associated with replication foci. This possibility is supported by the past findings that only a small fraction of CDC45 is stably bound to chromatin at any given time and that CDC45 frequently binds to licensed origins for lengthy periods without firing (Bauerschmidt et al., 2007; Terui et al., 2024). Whatever the cause, the lack of colocalization with replication foci was an advantage in the context of the current work, where CDC45 was selected because of its rate-limiting role in replication initiation rather than its association with replication foci. If CDC45 had strongly colocalized with replication foci, it would have simply recapitulated the results produced with PCNA and would not have been informative.

The observed CDC45 foci are also unlikely to be specific to replication initiation sites, as they were present throughout the cell cycle independent of replication or licensing. Segmentation of CDC45 foci was performed not to identify putative initiation sites but rather to reduce non-specific background signal, facilitate analysis with FOC-Map, and ensure methodological consistency with the approach used for replication foci to allow direct comparison of results. Our model uses the localization of CDC45 foci primarily as a tractable proxy for assessing relative initiation potential rather than direct

initiation events. Follow-up studies should seek to corroborate the localization observed here using orthogonal methods to visualize CDC45, ideally with endogenous labelling in live cells. No prior work has directly assessed the relationship between CDC45 and the PCH domain, although the figures in at least one prior work appear to display relatively little CDC45 within the DAPI-bright regions characteristic of PCH domains (Wong et al., 2011).

The role of HP1a, outstanding questions, and future directions

Although our experimental design does not enable any conclusions about HP1a's possible contribution to the observed dynamics, several pieces of evidence make it a promising candidate for further study of the spatio-temporal regulation of PCH replication. HP1a's central role in the organization and establishment of the PCH domain through condensate formation suggest that it may help to orchestrate the domain's exclusion of CDC45, and possibly of other replication factors whose localization with respect to the PCH domain have not yet been characterized. If HP1a is at least partially responsible for CDC45's exclusion, this could provide a mechanism for its documented modulation of PCH replication timing (Schwaiger et al., 2010; Yuan & O'Farrell, 2016). It would be informative to test whether depletion of HP1a lessens or abolishes CDC45's exclusion, particularly in comparison to perturbations that reduce the compaction of PCH without disrupting its recruitment of HP1a. Future work should also determine whether low levels of CDC45 are more highly correlated with HP1a than they are with chromatin compaction. It would also be of interest to assess whether artificially increasing CDC45 levels within the PCH domain would be sufficient to cause early replication of PCH, or an interspersed pattern of replication within the domain at times when replication would ordinarily be restricted to the periphery. Such a perturbation can be achieved by tagging CDC45 with one of the recently identified weakly binding variants of the HP1a interacting motif that could facilitate access to the domain without causing strong enrichment (Colmenares et al., 2025).

This work provides additional support for an emerging consensus that heterochromatin replication occurs not only at the outer periphery of the PCH domain, but also in locally decondensed internal regions. It additionally suggests that large scale relocalization of internal sequences to the surface of the domain may not be required for replication. At the same time, our study validates earlier observations of replication foci strongly enriched at the periphery of the PCH domain and is one of only two studies that situates this pattern within a consistent temporal sequence using time-lapse imaging in live cells. It also extends this understanding by suggesting a possible mechanistic framework that relates these spatio-temporal dynamics to the newly observed exclusion of CDC45 from the PCH domain. Future work should seek to validate these findings and explore the new questions they raise, particularly regarding HP1a's role in the exclusion of CDC45 from the PCH domain and the distribution of other replication initiation factors.

Methods

Transient transfection of S2R+ Drosophila cells

Cultured S2R+ cells (DGRC Stock 150; RRID:CVCL_Z831) in log-phase growth were resuspended in Schneider's Medium (Gibco Cat. 21720024) supplemented with 10% Fetal Bovine Serum (FBS) at a concentration of $1x10^6$ cells/mL. 8-well chamber slides (Ibidi Cat. 80826) were seeded with 200 uL of resuspended cells per chamber, and cells were allowed to recover and adhere overnight at 25°C. Cells were transfected the following day with plasmids containing mScarletI-PCNA and mEGFP-HP1a under the control of the Copia promoter (pCopia). Plasmid transfection was performed with TransIT-2020 (Mirus Cat. MIR 5400) transfection reagent using a modified version of the manufacturer's protocol. Briefly, each well was transfected with 100 ng of each plasmid (200 ng total) complexed with 0.2 μL of TransIt-2020 transfection reagent in 40 uL of Serum-Free Schneider's Medium. Transfection mixture was added dropwise after incubating at room temperature for 30 minutes.

Time-lapse image acquisition and processing

Time-lapse imaging was performed 48-72 h after transfection. Images were collected on a Zeiss LSM880 with a Plan-Apochromat 63×/1.4 NA Oil DIC M27 objective and an Airyscan Detector in Fast Mode. Cells in early S-phase with numerous dispersed PCNA foci were selected for imaging to allow subsequent progression through late S-phase to be captured. Z-stacks were collected every 30 mins for 12-16 h with 2x line averaging and frame-sequential channel-switching. A zoom of 4.0 was used with the SR "optimal" presets for frame size and Z-interval, giving voxel dimensions of 43 x 43 x 211 nm. Both channels were imaged with a pixel dwell time of 0.55 μs and Master Gain of 775 with the "MBS 488/561" main beam splitter. mScarletI-PCNA was excited with the 561 nm laser line at 0.7% power with the "BP 570-620 + LP 645" emission filter. mEGFP-HP1a was excited with the 488 nm laser line at 0.5% power with the "BP 420-480 + BP 495-550" emission filter. Images were deconvolved by 3D Airyscan Processing in Zen Black (Zen 2.3 SP1) using the default processing strength.

Segmentation of nuclei was done in Arivis Vision4D (version 3.6) by setting a threshold for diffuse nuclear HP1a, which is far above the cytoplasmic and extracellular background. Prior to segmentation, the HP1a channel was denoised with a discrete Gaussian filter with a diameter of 4.95 μm. Segmentation was then performed with the Watershed method, using a threshold of 150, a diameter of 8.75 μm, and a split sensitivity of 0.5%. Segments were then tracked to group the segments for each nucleus across timepoints. The segments for each nuclear track were then converted to saturated masks and exported as .ome.tiff files.

Nuclei were then normalized within a custom FIJI macro to reduce the effects of photobleaching and variability in expression levels between transfected cells. For the mEGFP-HP1a images, nuclear intensity values were divided by the average nuclear intensity at each timepoint, yielding the relative intensity of each nuclear voxel. For the mScarletI-PCNA channel, a single rescaling factor was calculated from the average mean nuclear intensity of the first three timepoints and applied uniformly to all timepoints. This approach was chosen to correct for differences in expression level

between cells while preserving changes in overall PCNA intensity. Following normalization, segmentation of PCNA foci from t was performed in Arivis Vision4D using an adaptive mean threshold with a diameter of 0.341 µm, a local threshold of 0.25, and 55% thinning.

To enable comparison between cells with different rates of S-phase progression, the time-lapse data from each cell were temporally aligned by expressing each timepoint as a percentage of the duration of late S-phase. The onset of late S-phase was identified by visual inspection as the timepoint at which PCNA foci converged at the PCH domain, and its completion was defined as the last timepoint at which segmented PCNA foci were present. Timepoints in early and mid S-phase precede the onset of late S-phase and therefore have negative progression values. From each time-lapse, the timepoints closest to -20%, 20%, 60%, and 100% progression through late S-phase were selected for subsequent analysis with FOC-Map.

Live cell FOC-Map analysis

As described in Chapter 2, FOC-Map was performed to quantify the distribution of replication foci with respect to the HP1a-rich PCH domain. FOC-Map processing was implemented in Matlab (Mathworks R2023b) using custom scripts. The normalized HP1a intensity images and binary PCNA foci masks produced by the preceding steps were used as inputs. Within each nucleus, voxels with HP1a intensity above the nuclear background were sorted into 1000 percentile intensity bins (0.1% increments from the 0th to 99.9th percentile), and the average HP1a intensity of voxels in each bin was recorded. Voxel coordinates were converted from image indices to nanometers using the Airyscan-processed voxel dimensions (42 × 42 × 211 nm) to account for anisotropic voxel geometry. For each voxel in a given percentile intensity bin, all nuclear voxels were binned by their distance from that voxel in 42 nm intervals. Within each distance bin, the total number of nuclear voxels and the number of segmented PCNA foci voxels were counted. This process was repeated for every voxel in the intensity bin, and the resulting counts were pooled across voxels within each distance bin. The procedure was then repeated for each percentile intensity bin. To generate pooled results for each timepoint, the nuclear voxel counts and PCNA foci voxel counts for each combination of intensity bin and distance bin were summed across all nuclei at that timepoint, as were the total PCNA foci and nuclear volumes. The FOC was then calculated from these pooled counts for each combination of intensity bin and distance bin. The average HP1a intensity for each percentile bin was recalculated from the pooled intensity values across all contributing nuclei.

For Figure 1B, the FOC values at zero distance (direct overlap) were extracted for each intensity bin and plotted against the corresponding average HP1a intensity, expressed as fold nuclear average. For Figure 1C, the full matrix of FOC values across all intensity and distance bins was displayed as a pseudocolor heatmap with HP1a intensity on the X-axis (scaled by average bin intensity rather than percentile rank), distance on the Y-axis, and FOC encoded as color. Percentile bins left empty due to limited bit-depth in the intensity values were excluded from the heatmap prior to plotting. Heatmaps were plotted using interpolated shading with a color scale range of 0 to 25.

EdU-labelling and immunofluorescence

Clean and sterile coverslips (22x22mm 1.5H) were incubated in 100% Fetal Bovine Serum (FBS) for 2 h at 37°C to facilitate adsorption of extracellular matrix components and promote cell adherence. After rinsing with 1x PBS, coverslips were transferred to 6-well plates and seeded with 2 mL of $1x10^6$ S2R+ cells/mL in Schneider's Medium supplemented with 10% FBS. Cells were allowed to adhere overnight at 25°C. The following day, cells were treated with 10 μM EdU in conditioned medium for five minutes, fixed for five minutes in 4% paraformaldehyde (PFA) in 1x PBS, then permeabilized and washed in 1xPBS + 0.4% TritonX-100 (PBST) three times for five minutes. Residual fixation was quenched by incubation in blocking buffer (1x PBST + 5% FBS) for one hour at room temp. Labelling with Alexa647 picolyl azide was performed with the Click-iT Plus kit (Invitrogen Cat. C10640) according to the manufacturer's protocol, but the Click-labeling step was performed twice to increase the signal and compensate for the brief duration of pulse-labeling. After labeling, fixed coverslips were stored overnight in blocking buffer at 4°C.

Coverslips were then incubated at 4°C with blocking buffer containing 1 μg/mL monoclonal mouse anti-HP1a (C1A9 from DGRC) and a 1:400 dilution of affinity purified rabbit anti-CDC45 , which was kindly provided by Mike Botchan and has been validated to recognize CDC45 within the fully assembled CMG complex (Moyer et al., 2006). Primary antibody incubation was continued overnight at 4°C followed by 3x 5 min washes in room temperature PBST. Secondary antibody staining was done with 1:500 dilutions of Alexa 568 goat anti-mouse (2 mg/mL; Invitrogen Cat. A21202) and Alexa488 goat anti-rabbit (2 mg/mL; Invitrogen Cat. A11034)) in blocking buffer incubated at room temperature for 90 minutes. Coverslips were again washed 3x 5 minutes in PBST, then post-fixed in 4% PFA in 1x PBST for 5 minutes. PFA was then washed off with 3x 5 min incubations in PBST and quenched in blocking buffer for 1 hour. Nuclei were counter-stained with DAPI in 1x PBS for five minutes, quickly rinsed in 1xPBS, and mounted on slides with SlowFade Glass (Thermo Cat. S36917). Mounted slides were sealed with nail polish and stored at -20°C before imaging.

Fixed cell image acquisition and processing

Z-stacks were acquired on the Zeiss LSM880 with a Plan-Apochromat 63×/1.4 NA Oil DIC M27 objective and an Airyscan Detector in Superresolution mode. Images were acquired using 2x line averaging and frame-sequential channel-switching with a pixel dwell time of 1.04 μs, a zoom of 7.5, and the optimal frame size in SR mode, giving voxel dimensions of 35 x 35 x 159 nm. All channels were imaged with a master gain of 800 and bit-depth of 16 with the MBS 488/561/633 and MBS-405 main beam splitters. The SBS LP 660 secondary beam splitter was used only when imaging Alexa647-EdU to prevent bleed-through from Alexa568. Alexa647-EdU was excited with the 633 nm laser at 2% power with the BP 570-670 + LP 645 emission filter. Alexa568-labeled anti-HP1a was excited with the 561 nm laser line at 0.3% power using the BP 420-480 + BP 495-620 emission filter. Alexa488-labelled anti-CDC45 was excited with the 488 nm laser line at 0.5% power. DAPI was excited with the 405 nm laser at 0.2% power and the BP 420-480 + BP 495-550 emission filter.

Images were deconvolved by 3D Airyscan Processing (SR Mode) using processing strengths of 7.3 for Alexa647-EdU, 7.5 for Alexa568-HP1a, 7.0 for Alexa488-CDC45, and 7.0 for DAPI in Zen 2.3 Blue Edition. Chromatic aberration was measured from images of a tetraspeck bead slide acquired with the same settings used for fixed cells. After airyscan processing, the shifts between channels were by corrected by lateral channel alignment in Zen Black using the average shifts measured from three bead images. After correction of chromatic aberration, nuclear segmentation was performed in Arivis Vision4D. The HP1a and DAPI channels were each smoothed with a discrete Gaussian filter (4 μm diameter), summed, and the resulting combined image was segmented using the Otsu method.

Background correction and normalization of fixed-cell images were performed with a custom Fiji macro. A constant background intensity was estimated independently for each channel using a conservative approach based on the minimum local average intensity in the image. The top five and bottom twenty z-slices were excluded to avoid edge artifacts from Airyscan processing and elevated background near the coverslip surface. A mean filter was applied in XY (radius of 20 pixels) and in Z (radius of 2 slices), and the resulting smoothed stack was reduced by minimum-intensity z-projection. The minimum value in the projection was taken as the estimated background for each channel and subtracted as a constant from all voxels, with any resulting negative values set to zero. The HP1a channel was normalized by dividing nuclear voxel intensities by the mean nuclear intensity, yielding relative intensity values as described for the live-cell images. To enable consistent segmentation of foci across cells with varying absolute intensities, the EdU and CDC45 channels were linearly rescaled within each nucleus such that the maximum nuclear voxel intensity was set to a fixed standard of 10,000. Segmentation of EdU and CDC45 foci was then performed in Arivis Vision4D using the adaptive mean method with a diameter of 0.213 μm, a local threshold of 750, and 55% thinning. The resulting segments were converted to saturated masks and exported as OME-TIFF files.

Classification of cell cycle phase in fixed cells

Cells in S-phase were distinguished from G-phase cells by the presence of EdU foci. Cells in each image were manually annotated as being in early or late S-phase using roughly the same strategy as in live cells, where cells with numerous dispersed replication foci were annotated as being in early or mid S-phase, while those with a smaller number of replication foci near the PCH domain were classified as being in late S-phase. Cell cycle classification was checked against the count of segmented replication foci and integrated DAPI signal, which both correlated well with S-phase progression, with manual staging being used to more accurately classify the few outliers where cell cycle stage was not captured by these more objective methods.

G-phase cells were classified as G1 or G2 based on integrated nuclear DAPI intensity, which serves as a proxy for total DNA content. A histogram of integrated DAPI among G-phase cells revealed a clear bimodal distribution, with one peak between 50 and 59 million arbitrary units and a second peak between 100 and 119 million arbitrary units, consistent with pre- and post-replication DNA content respectively. Of the 228 cells for that were classified for cell cycle stage, 4 EdU-negative (G-phase) were

excluded from analysis because their DNA content fell between the two peaks and did not permit a reliable classification as G1 or G2.

FOC-Map analysis of fixed cells

FOC-Map analysis of fixed-cell images was performed using the same approach described for live-cell time-lapse data, with modifications to account for differences in image acquisition parameters and experimental design. The analysis was implemented in custom MATLAB scripts and followed the same computational workflow of percentile intensity binning, distance binning, and calculation of the Fractional Overlap Coefficient (FOC) described in Chapter 2. HP1a intensity within each nucleus was normalized to the mean nuclear value, as was done for live cells. Percentile intensity bins of 0.05% were used (compared to 0.1% for live cells), and distance bins were set to 35.42 nm, matching the lateral voxel dimensions of the fixed-cell Airyscan images. The analysis was performed independently for EdU foci and CDC45 foci, each measured against the HP1a channel, using the binary foci masks generated during segmentation.

Rather than aligning cells by temporal progression through late S-phase as was done for live-cell time-lapse data, fixed cells were grouped by cell-cycle stage and pooled within each group. Pooling was performed by summing the raw voxel counts for each combination of intensity and distance bin across all cells in a given stage prior to calculating the FOC, following the same pooling strategy used for live cells. The resulting FOC-Maps represent the aggregate spatial relationship between foci and the HP1a-labeled PCH domain for each cell-cycle stage.

Acknowledgements

Sincere thanks to all members of the Karpen lab for feedback and guidance. Thanks to Mike Botchan for sharing antibodies against CDC45 and other replication factors, and to Serafin Colmenares for the plasmids used in transient transfections. This work was supported by funding from the National Institutes of Health (grant numbers R01 GM117420, T32 HG000047, T32 GM132022 and R35 GM139653).

CHAPTER 4

General discussion and future directions

The faithful replication of heterochromatin is essential for genome stability and chromosome segregation, yet the mechanisms governing when and where heterochromatin replication occurs remain incompletely understood. Progress in this area has been constrained in part by the analytical challenges posed by the PCH domain's irregular morphology, and limited spatial and temporal resolution applied in prior studies.

FOC-Map as a tool for the analysis and visualization of spatial relationships in multichannel images

FOC-Map was developed to address the challenges encountered in our analysis of PCH replication, but its modular design allows it to be modified and optimized for projects with different needs. At the same time, the problems it was designed to overcome are common in cellular biology and not unique to this study. By requiring segmentation of only one channel and replacing threshold-based definitions of the other with percentile intensity binning, FOC-Map avoids many of the arbitrary decisions that complicate analysis of such images. Studies of chromatin, condensates, or any intracellular bodies with irregular morphology and poorly defined boundaries are likely to benefit from the reduced reliance on segmentation, especially when inconsistencies in segmentation can obscure the signal that is being measured or visualized. FOC-Map may also be of value for imaging-based studies of structures that share an interface, as this often produces non-monotonic relationships that are problematic for pixel-based approaches, and make the result highly dependent on thresholding if an object-based approach is used. Finally, FOC-Map is particularly well-suited to studies where exclusion and enrichment must both be measured using a single approach, as PCC suffers from a bias toward positive values, while object-based approaches generally show the absence of colocalization rather than the presence of exclusion or depletion (Barlow et al., 2010; Moser et al., 2017). Several extensions of the method may further strengthen its utility. The current implementation pools data across cells to reduce noise, but does not include a statistical framework for assessing significance or estimating uncertainty across pooled bins. Future work should also incorporate a statistical approach to estimate uncertainty within bins and enable significance testing in comparisons between bins or between plots.

Dynamics and organization of PCH replication

Previous studies of heterochromatin replication in mammalian cells produced two distinct models for where replication occurs relative to the PCH domain. The first proposed that heterochromatic sequences must translocate to the surface of the domain in order to be replicated, based on the observation that replication foci in late S-phase were restricted to a ring-like pattern at the domain periphery (Quivy et al., 2004). Subsequent work using higher-resolution imaging and live-cell approaches found that replication also occurs within less compacted regions inside the domain, leading to an

alternative model in which local decondensation permits replication without large-scale movement of chromatin to the surface (Chagin et al., 2019; Markaki et al., 2012). Our results in cultured *Drosophila* cells are broadly consistent with this latter model. Replication foci were initially restricted to the periphery of the PCH domain at the onset of late S-phase but were later observed within low-HP1a channels interspersed throughout its interior, with no indication that internal sequences needed to relocate to the domain surface. These findings add to a growing body of evidence favoring local decondensation as the primary mode by which heterochromatic sequences within the PCH domain are replicated. One limitation of the present work is that the temporal resolution of our time-lapse imaging cannot fully exclude the possibility that transient, localized decondensation immediately precedes replication at individual sites, rendering chromatin accessible on a timescale shorter than our imaging intervals. Addressing this would require higher temporal resolution or alternative approaches capable of capturing such rapid transitions.

The model proposed in Chapter 3 suggests that the depletion of CDC45 within the PCH domain limits replication initiation in its interior, confining the onset of heterochromatin replication to the domain's periphery and giving rise to the outside-in progression observed in our time-lapse data. If corroborated, this mechanism would provide a unifying explanation for both the spatial and temporal dynamics of PCH replication, linking the characteristic delay in heterochromatin replication timing to the spatial organization of the domain itself. Rather than treating timing and spatial organization as independent features of heterochromatin replication, the model frames them as coupled consequences of the same underlying constraint on initiation. How this mechanism interacts with other known regulators of replication timing, such as RIF1-mediated antagonism of DDK activity and potential differences in origin licensing density, remains an open question that warrants further investigation.

If CDC45's depletion within the PCH domain reflects biophysical properties of the domain such as selective permeability or affinity partitioning, it is likely that other factors required for replication initiation are similarly affected. The assembly of a functional CMG helicase at a licensed origin requires the coordinated recruitment of multiple components, and the partial exclusion of even a few of these would be expected to produce a synergistic reduction in the rate of origin firing within the domain. Future work should assess the distribution of additional initiation factors relative to the PCH domain, and the combined effects of their depletion should be modeled more quantitatively to determine whether the magnitude of exclusion observed for CDC45 alone is sufficient to account for the near-complete absence of replication foci from the domain interior at the onset of late S-phase, or whether the exclusion of multiple factors is required.

A central question raised by these findings is whether HP1a itself, through its role in organizing the PCH domain and establishing its condensate-like properties, is responsible for the exclusion of CDC45. HP1a is essential for the formation of the PCH domain (Strom et al., 2017) and has been shown to delay the replication of sequences it is targeted to in *Drosophila* embryos (Yuan & O'Farrell, 2016). If depletion of HP1a were found to restore CDC45 access to heterochromatic regions, this could provide a mechanistic basis for HP1a's observed influence on replication timing, connecting a well-documented but poorly understood phenotype to a specific effect on the distribution

of a rate-limiting initiation factor. However, HP1a depletion would also disrupt numerous other aspects of heterochromatin organization, making it difficult to attribute changes in CDC45 distribution or replication dynamics specifically to the loss of condensate properties. Approaches that perturb the biophysical properties of the domain without fully eliminating HP1a would be valuable in this regard, as they could more directly test whether the condensate-like features of the domain are responsible for CDC45's exclusion and whether altering these properties is sufficient to change replication dynamics. To this end, it would be of interest to test the effect of HP1a mutations that alter condensate properties in differing ways (Brennan et al., 2026).

A complementary approach would be to test whether targeting CDC45 to the PCH domain is sufficient to alter the spatial or temporal dynamics of replication. As suggested in Chapter 3, this might be achieved by fusing CDC45 to a weakly interacting HP1a-binding motif designed to facilitate access to the domain without causing artificial enrichment beyond the level in the nucleosol. If this manipulation accelerated heterochromatin replication or allowed replication foci to form within the domain interior at the onset of late S-phase, it would provide direct functional evidence that CDC45 exclusion is a meaningful constraint on replication initiation within the domain. Such an experiment would also help to isolate the contribution of CDC45 from other variables that may influence heterochromatin replication timing, including RIF1-mediated regulation of origin activation, potential differences in origin licensing, and the possible exclusion of other replication factors that have not yet been characterized.

More broadly, the possibility that the biophysical properties of the PCH domain influence the distribution of replication factors connects this work to ongoing efforts to understand how condensate properties relate to biological function (Alberti et al., 2019; Lyon et al., 2021). In many systems where phase separation or similar mechanisms have been implicated, it remains difficult to determine whether the material properties of a compartment are functionally relevant or incidental. Heterochromatin replication may therefore provide a unique window into these questions.

References

Aaron, J. S., Taylor, A. B., & Chew, T.-L. (2018). Image co-localization – co-occurrence versus correlation. *Journal of Cell Science*, *131*(3). https://doi.org/10.1242/jcs.211847

Adler, J., Pagakis, S. N., & Parmryd, I. (2008). Replicate-based noise corrected correlation for accurate measurements of colocalization. *Journal of Microscopy*, *230*(1), 121–133. https://doi.org/10.1111/j.1365-2818.2008.01967.x

Adler, J., & Parmryd, I. (2010). Quantifying colocalization by correlation: The Pearson correlation coefficient is superior to the Mander's overlap coefficient. *Cytometry Part A*, *77A*(8), 733–742. https://doi.org/10.1002/cyto.a.20896

Alberti, S., Gladfelter, A., & Mittag, T. (2019). Considerations and Challenges in Studying Liquid-Liquid Phase Separation and Biomolecular Condensates. *Cell*, *176*(3), 419–434. https://doi.org/10.1016/j.cell.2018.12.035

Allshire, R. C., & Madhani, H. D. (2018). Ten principles of heterochromatin formation and function. *Nature Reviews Molecular Cell Biology*, *19*(4), 229–244. https://doi.org/10.1038/nrm.2017.119

Aparicio, O. M., Weinstein, D. M., & Bell, S. P. (1997). Components and Dynamics of DNA Replication Complexes in S. cerevisiae: Redistribution of MCM Proteins and Cdc45p during S Phase. *Cell*, *91*(1), 59–69. https://doi.org/10.1016/S0092-8674(01)80009-X

Barlow, A. L., MacLeod, A., Noppen, S., Sanderson, J., & Guérin, C. J. (2010). Colocalization Analysis in Fluorescence Micrographs: Verification of a More

Accurate Calculation of Pearson's Correlation Coefficient. *Microscopy and Microanalysis*, *16*(6), 710–724. https://doi.org/10.1017/S143192761009389X

Bauerschmidt, C., Pollok, S., Kremmer, E., Nasheuer, H., & Grosse, F. (2007). Interactions of human Cdc45 with the Mcm2–7 complex, the GINS complex, and DNA polymerases δ and ε during S phase. *Genes to Cells*, *12*(6), 745–758. https://doi.org/10.1111/j.1365-2443.2007.01090.x

Blumenthal, A. B., Kriegstein, H. J., & Hogness, D. S. (1974). The Units of DNA Replication in Drosophila melanogaster Chromosomes. *Cold Spring Harbor Symposia on Quantitative Biology*, *38*(0), 205–223. https://doi.org/10.1101/SQB.1974.038.01.024

Bolte, S., & Cordelières, F. P. (2006). A guided tour into subcellular colocalization analysis in light microscopy. *Journal of Microscopy*, *224*(3), 213–232. https://doi.org/10.1111/j.1365-2818.2006.01706.x

Bravo, R., & Macdonald-Bravo, H. (1987). Existence of two populations of cyclin/proliferating cell nuclear antigen during the cell cycle: Association with DNA replication sites. *The Journal of Cell Biology*, *105*(4), 1549–1554. https://doi.org/10.1083/jcb.105.4.1549

Brennan, L. D., Kim, H.-K., Colmenares, S., Ego, T., Ryu, J.-K., & Karpen, G. (2026). *In vitro* reconstitution of heterochromatin compartments reveals the spontaneous formation of tunable liquid–liquid interfaces. *Nucleic Acids Research*, *54*(5), gkag201. https://doi.org/10.1093/nar/gkag201

Broderick, R. (2012). *Protein-protein interactions, sub-cellular localisation and mobility of the human Cdc45 protein.* [Doctoral thesis, University of Galway]. https://doi.org/10.13025/16945

Chagin, V. O., Reinhart, B., Becker, A., Mortusewicz, O., Jost, K. L., Rapp, A., Leonhardt, H., & Cardoso, M. C. (2019). Processive DNA synthesis is associated with localized decompaction of constitutive heterochromatin at the sites of DNA replication and repair. *Nucleus*, *10*(1), 231–253. https://doi.org/10.1080/19491034.2019.1688932

Chen, N., & Buonomo, S. C. B. (2023). Three-dimensional nuclear organisation and the DNA replication timing program. *Current Opinion in Structural Biology*, *83*, 102704. https://doi.org/10.1016/j.sbi.2023.102704

Chiolo, I., Minoda, A., Colmenares, S. U., Polyzos, A., Costes, S. V., & Karpen, G. H. (2011). Double-Strand Breaks in Heterochromatin Move Outside of a Dynamic HP1a Domain to Complete Recombinational Repair. *Cell*, *144*(5), 732–744. https://doi.org/10.1016/j.cell.2011.02.012

Cho, C.-Y., Seller, C. A., & O'Farrell, P. H. (2022a). Temporal control of late replication and coordination of origin firing by self-stabilizing Rif1-PP1 hubs in *Drosophila*. *Proceedings of the National Academy of Sciences*, *119*(26). https://doi.org/10.1073/pnas.2200780119

Cho, C.-Y., Seller, C. A., & O'Farrell, P. H. (2022b). Temporal control of late replication and coordination of origin firing by self-stabilizing Rif1-PP1 hubs in *Drosophila*. *Proceedings of the National Academy of Sciences*, *119*(26), e2200780119. https://doi.org/10.1073/pnas.2200780119

Ciardo, D., Goldar, A., & Marheineke, K. (2019). On the Interplay of the DNA Replication Program and the Intra-S Phase Checkpoint Pathway. *Genes*, *10*(2), 94. https://doi.org/10.3390/genes10020094

Colmenares, S. U., Tsukamoto, S., Hickmann, C., Brennan, L. D., Khavani, M., Mofrad, M. R. K., & Karpen, G. H. (2025). Expanding the HP1a-binding consensus and molecular grammar for heterochromatin assembly. *Nucleic Acids Research*, *53*(19), gkaf976. https://doi.org/10.1093/nar/gkaf976

Cordelières, F. P., & Bolte, S. (2014). Experimenters' guide to colocalization studies. In *Methods in Cell Biology* (pp. 395–408). Elsevier. https://doi.org/10.1016/b978-0-12-420138-5.00021-5

Costa, A., & Diffley, J. F. X. (2022). The Initiation of Eukaryotic DNA Replication. *Annual Review of Biochemistry*, *91*(1), 107–131. https://doi.org/10.1146/annurev-biochem-072321-110228

Dernburg, A. F., Sedat, J. W., & Hawley, R. S. (1996). Direct Evidence of a Role for Heterochromatin in Meiotic Chromosome Segregation. *Cell*, *86*(1), 135–146. https://doi.org/10.1016/S0092-8674(00)80084-7

Dimitrova, D. S., Todorov, I. T., Melendy, T., & Gilbert, D. M. (1999). Mcm2, but Not Rpa, Is a Component of the Mammalian Early G1-Phase Prereplication Complex. *The Journal of Cell Biology*, *146*(4), 709–722. https://doi.org/10.1083/jcb.146.4.709

Dunn, K. W., Kamocka, M. M., & McDonald, J. H. (2011). A practical guide to evaluating colocalization in biological microscopy. *American Journal of Physiology-Cell Physiology*, *300*(4), C723–C742. https://doi.org/10.1152/ajpcell.00462.2010

Edwards, M. C., Tutter, A. V., Cvetic, C., Gilbert, C. H., Prokhorova, T. A., & Walter, J. C. (2002). MCM2–7 Complexes Bind Chromatin in a Distributed Pattern Surrounding the Origin Recognition Complex inXenopus Egg Extracts. *Journal of Biological Chemistry*, *277*(36), 33049–33057. https://doi.org/10.1074/jbc.M204438200

Elgin, S. C. R., & Reuter, G. (2013). Position-Effect Variegation, Heterochromatin Formation, and Gene Silencing in Drosophila. *Cold Spring Harbor Perspectives in Biology*, *5*(8), a017780–a017780. https://doi.org/10.1101/cshperspect.a017780

Fan, Y., Köberlin, M. S., Ratnayeke, N., Liu, C., Deshpande, M., Gerhardt, J., & Meyer, T. (2021). LRR1-mediated replisome disassembly promotes DNA replication by recycling replisome components. *Journal of Cell Biology*, *220*(8), e202009147. https://doi.org/10.1083/jcb.202009147

Fragkos, M., Ganier, O., Coulombe, P., & Méchali, M. (2015). DNA replication origin activation in space and time. *Nature Reviews Molecular Cell Biology*, *16*(6), 360–374. https://doi.org/10.1038/nrm4002

French, A. P., Mills, S., Swarup, R., Bennett, M. J., & Pridmore, T. P. (2008). Colocalization of fluorescent markers in confocal microscope images of plant cells. *Nature Protocols*, *3*(4), 619–628. https://doi.org/10.1038/nprot.2008.31

Gelléri, M., Sterr, M., Strickfaden, H., Cremer, C., Cremer, T., & Cremer, M. (2024). *Space-time dynamics of genome replication studied with super-resolved microscopy*. Cell Biology. https://doi.org/10.1101/2024.03.22.586000

Goldar, A., Marsolier-Kergoat, M.-C., & Hyrien, O. (2009). Universal Temporal Profile of Replication Origin Activation in Eukaryotes. *PLoS ONE*, *4*(6), e5899. https://doi.org/10.1371/journal.pone.0005899

Hoskins, R. A., Carlson, J. W., Kennedy, C., Acevedo, D., Evans-Holm, M., Frise, E., Wan, K. H., Park, S., Mendez-Lago, M., Rossi, F., Villasante, A., Dimitri, P., Karpen, G. H., & Celniker, S. E. (2007). Sequence Finishing and Mapping of *Drosophila melanogaster* Heterochromatin. *Science*, *316*(5831), 1625–1628. https://doi.org/10.1126/science.1139816

Hu, Y., & Stillman, B. (2023). Origins of DNA replication in eukaryotes. *Molecular Cell*, *83*(3), 352–372. https://doi.org/10.1016/j.molcel.2022.12.024

Hyrien, O. (2015). Peaks cloaked in the mist: The landscape of mammalian replication origins. *Journal of Cell Biology*, *208*(2), 147–160. https://doi.org/10.1083/jcb.201407004

Ibarra, A., Schwob, E., & Méndez, J. (2008). Excess MCM proteins protect human cells from replicative stress by licensing backup origins of replication. *Proceedings of the National Academy of Sciences*, *105*(26), 8956–8961. https://doi.org/10.1073/pnas.0803978105

Ilves, I., Petojevic, T., Pesavento, J. J., & Botchan, M. R. (2010). Activation of the MCM2-7 Helicase by Association with Cdc45 and GINS Proteins. *Molecular Cell*, *37*(2), 247–258. https://doi.org/10.1016/j.molcel.2009.12.030

Janssen, A., Colmenares, S. U., & Karpen, G. H. (2018). Heterochromatin: Guardian of the Genome. *Annual Review of Cell and Developmental Biology*, *34*(1), 265–288. https://doi.org/10.1146/annurev-cellbio-100617-062653

Jensen, S., Gassama, M.-P., & Heidmann, T. (1999). Taming of transposable elements by homology-dependent gene silencing. *Nature Genetics*, *21*(2), 209–212. https://doi.org/10.1038/5997

Katsuno, Y., Suzuki, A., Sugimura, K., Okumura, K., Zineldeen, D. H., Shimada, M., Niida, H., Mizuno, T., Hanaoka, F., & Nakanishi, M. (2009). Cyclin A–Cdk1 regulates the origin firing program in mammalian cells. *Proceedings of the National Academy of Sciences*, *106*(9), 3184–3189. https://doi.org/10.1073/pnas.0809350106

Klosin, A., & Hyman, A. A. (2017). A liquid reservoir for silent chromatin. *Nature*, *547*(7662), 168–169. https://doi.org/10.1038/nature23089

Köhler, C., Koalick, D., Fabricius, A., Parplys, A. C., Borgmann, K., Pospiech, H., & Grosse, F. (2016). Cdc45 is limiting for replication initiation in humans. *Cell Cycle*, *15*(7), 974–985. https://doi.org/10.1080/15384101.2016.1152424

Lachner, M., O'Carroll, D., Rea, S., Mechtler, K., & Jenuwein, T. (2001). Methylation of histone H3 lysine 9 creates a binding site for HP1 proteins. *Nature*, *410*(6824), 116–120. https://doi.org/10.1038/35065132

Larson, A. G., Elnatan, D., Keenen, M. M., Trnka, M. J., Johnston, J. B., Burlingame, A. L., Agard, D. A., Redding, S., & Narlikar, G. J. (2017). Liquid droplet formation by HP1α suggests a role for phase separation in heterochromatin. *Nature*, *547*(7662), 236–240. https://doi.org/10.1038/nature22822

Larson, A. G., & Narlikar, G. J. (2018). The Role of Phase Separation in Heterochromatin Formation, Function, and Regulation. *Biochemistry*, *57*(17), 2540–2548. https://doi.org/10.1021/acs.biochem.8b00401

Lima-de-Faria, A. (1959). Differential Uptake of Tritiated Thymidine into Hetero- and Euchromatin in *Melanoplus* and *Secale*. *The Journal of Cell Biology*, *6*(3), 457–466. https://doi.org/10.1083/jcb.6.3.457

Lima-De-Faria, A., & Jaworska, H. (1968). Late DNA Synthesis in Heterochromatin. *Nature*, *217*(5124), 138–142. https://doi.org/10.1038/217138a0

Loebel, D., Huikeshoven, H., & Cotterill, S. (2000). Localisation of the DmCdc45 DNA replication factor in the mitotic cycle and during chorion gene amplification. *Nucleic Acids Research*, *28*(20), 3897–3903. https://doi.org/10.1093/nar/28.20.3897

Lu, B. Y., Emtage, P. C. R., Duyf, B. J., Hilliker, A. J., & Eissenberg, J. C. (2000). Heterochromatin Protein 1 Is Required for the Normal Expression of Two Heterochromatin Genes in Drosophila. *Genetics*, *155*(2), 699–708. https://doi.org/10.1093/genetics/155.2.699

Lyon, A. S., Peeples, W. B., & Rosen, M. K. (2021). A framework for understanding the functions of biomolecular condensates across scales. *Nature Reviews Molecular Cell Biology*, *22*(3), 215–235. https://doi.org/10.1038/s41580-020-00303-z

MacAlpine, H. K., Gordân, R., Powell, S. K., Hartemink, A. J., & MacAlpine, D. M. (2010). *Drosophila* ORC localizes to open chromatin and marks sites of cohesin complex loading. *Genome Research*, *20*(2), 201–211. https://doi.org/10.1101/gr.097873.109

Manders, E. M. M., Stap, J., Brakenhoff, G. J., Driel, R. V., & Aten, J. A. (1992). Dynamics of three-dimensional replication patterns during the s-phase, analysed

by double labelling of dna and confocal microscopy. *Journal of Cell Science*, *103*(3), 857–862. https://doi.org/10.1242/jcs.103.3.857

Manders, E. M. M., Verbeek, F. J., & Aten, J. A. (1993). Measurement of co-localization of objects in dual-colour confocal images. *Journal of Microscopy*, *169*(3), 375–382. https://doi.org/10.1111/j.1365-2818.1993.tb03313.x

Marchal, C., Sima, J., & Gilbert, D. M. (2019). Control of DNA replication timing in the 3D genome. *Nature Reviews Molecular Cell Biology*, *20*(12), 721–737. https://doi.org/10.1038/s41580-019-0162-y

Marinsek, N. (2010). *Human GINS, a conserved DNA replication factor and candidate cancer marker* [Apollo - University of Cambridge Repository]. https://doi.org/10.17863/CAM.16510

Markaki, Y., Smeets, D., Fiedler, S., Schmid, V. J., Schermelleh, L., Cremer, T., & Cremer, M. (2012). The potential of 3D-FISH and super-resolution structured illumination microscopy for studies of 3D nuclear architecture: 3D structured illumination microscopy of defined chromosomal structures visualized by 3D (immuno)-FISH opens new perspectives for studies of nuclear architecture. *BioEssays*, *34*(5), 412–426. https://doi.org/10.1002/bies.201100176

Mei, L., Kedziora, K. M., Song, E.-A., Purvis, J. E., & Cook, J. G. (2022). The consequences of differential origin licensing dynamics in distinct chromatin environments. *Nucleic Acids Research*, *50*(17), 9601–9620. https://doi.org/10.1093/nar/gkac003

Menolfi, D., Lee, B. J., Zhang, H., Jiang, W., Bowen, N. E., Wang, Y., Zhao, J., Holmes, A., Gershik, S., Rabadan, R., Kim, B., & Zha, S. (2023). ATR kinase supports

normal proliferation in the early S phase by preventing replication resource exhaustion. *Nature Communications*, *14*(1), 3618. https://doi.org/10.1038/s41467-023-39332-5

Miotto, B., Ji, Z., & Struhl, K. (2016). Selectivity of ORC binding sites and the relation to replication timing, fragile sites, and deletions in cancers. *Proceedings of the National Academy of Sciences*, *113*(33). https://doi.org/10.1073/pnas.1609060113

Moiseeva, T. N., Yin, Y., Calderon, M. J., Qian, C., Schamus-Haynes, S., Sugitani, N., Osmanbeyoglu, H. U., Rothenberg, E., Watkins, S. C., & Bakkenist, C. J. (2019). An ATR and CHK1 kinase signaling mechanism that limits origin firing during unperturbed DNA replication. *Proceedings of the National Academy of Sciences*, *116*(27), 13374–13383. https://doi.org/10.1073/pnas.1903418116

Moser, B., Hochreiter, B., Herbst, R., & Schmid, J. A. (2017). Fluorescence colocalization microscopy analysis can be improved by combining object-recognition with pixel-intensity-correlation. *Biotechnology Journal*, *12*(1), 1600332. https://doi.org/10.1002/biot.201600332

Moyer, S. E., Lewis, P. W., & Botchan, M. R. (2006). Isolation of the Cdc45/Mcm2–7/GINS (CMG) complex, a candidate for the eukaryotic DNA replication fork helicase. *Proceedings of the National Academy of Sciences*, *103*(27), 10236–10241. https://doi.org/10.1073/pnas.0602400103

Nakamura, H., Morita, T., & Sato, C. (1986). Structural organizations of replicon domains during DNA synthetic phase in the mammalian nucleus. *Experimental Cell Research*, *165*(2), 291–297. https://doi.org/10.1016/0014-4827(86)90583-5

Parker, M. W., Botchan, M. R., & Berger, J. M. (2017). Mechanisms and regulation of DNA replication initiation in eukaryotes. *Critical Reviews in Biochemistry and Molecular Biology*, *52*(2), 107–144. https://doi.org/10.1080/10409238.2016.1274717

Polasek-Sedlackova, H., Miller, T. C. R., Krejci, J., Rask, M.-B., & Lukas, J. (2022). Solving the MCM paradox by visualizing the scaffold of CMG helicase at active replisomes. *Nature Communications*, *13*(1), 6090. https://doi.org/10.1038/s41467-022-33887-5

Powell, S. K., MacAlpine, H. K., Prinz, J. A., Li, Y., Belsky, J. A., & MacAlpine, D. M. (2015). Dynamic loading and redistribution of the Mcm2-7 helicase complex through the cell cycle. *The EMBO Journal*, *34*(4), 531–543. https://doi.org/10.15252/embj.201488307

Priest, JeanH. (1968). The replication of human heterochromatin in serial culture. *Chromosoma*, *24*(4). https://doi.org/10.1007/BF00285018

Quivy, J.-P., Roche, D., Kirschner, D., Tagami, H., Nakatani, Y., & Almouzni, G. (2004). A CAF-1 dependent pool of HP1 during heterochromatin duplication. *The EMBO Journal*, *23*(17), 3516–3526. https://doi.org/10.1038/sj.emboj.7600362

Rhind, N., Yang, S. C.-H., & Bechhoefer, J. (2010). Reconciling stochastic origin firing with defined replication timing. *Chromosome Research*, *18*(1), 35–43. https://doi.org/10.1007/s10577-009-9093-3

Richards, L., Das, S., & Nordman, J. T. (2022). Rif1-Dependent Control of Replication Timing. *Genes*, *13*(3), 550. https://doi.org/10.3390/genes13030550

Schwaiger, M., Kohler, H., Oakeley, E. J., Stadler, M. B., & Schübeler, D. (2010). Heterochromatin protein 1 (HP1) modulates replication timing of the *Drosophila* genome. *Genome Research*, *20*(6), 771–780. https://doi.org/10.1101/gr.101790.109

Seller, C. A., & O'Farrell, P. H. (2018). Rif1 prolongs the embryonic S phase at the Drosophila mid-blastula transition. *PLOS Biology*, *16*(5), e2005687. https://doi.org/10.1371/journal.pbio.2005687

Shermoen, A. W., McCleland, M. L., & O'Farrell, P. H. (2010). Developmental Control of Late Replication and S Phase Length. *Current Biology*, *20*(23), 2067–2077. https://doi.org/10.1016/j.cub.2010.10.021

Strom, A. R., Emelyanov, A. V., Mir, M., Fyodorov, D. V., Darzacq, X., & Karpen, G. H. (2017). Phase separation drives heterochromatin domain formation. *Nature*, *547*(7662), 241–245. https://doi.org/10.1038/nature22989

Tanaka, S., Nakato, R., Katou, Y., Shirahige, K., & Araki, H. (2011). Origin Association of Sld3, Sld7, and Cdc45 Proteins Is a Key Step for Determination of Origin-Firing Timing. *Current Biology*, *21*(24), 2055–2063. https://doi.org/10.1016/j.cub.2011.11.038

Terui, R., Berger, S. E., Sambel, L. A., Song, D., & Chistol, G. (2024). Single-molecule imaging reveals the mechanism of bidirectional replication initiation in metazoa. *Cell*, *187*(15), 3992-4009.e25. https://doi.org/10.1016/j.cell.2024.05.024

Wallrath, L. L., & Elgin, S. C. (1995). Position effect variegation in Drosophila is associated with an altered chromatin structure. *Genes & Development*, *9*(10), 1263–1277. https://doi.org/10.1101/gad.9.10.1263

Walter, H., & Brooks, D. E. (1995). Phase separation in cytoplasm, due to macromolecular crowding, is the basis for microcompartmentation. *FEBS Letters*, *361*(2–3), 135–139. https://doi.org/10.1016/0014-5793(95)00159-7

Wang, D., Zhou, J., Liu, X., Lu, D., Shen, C., Du, Y., Wei, F.-Z., Song, B., Lu, X., Yu, Y., Wang, L., Zhao, Y., Wang, H., Yang, Y., Akiyama, Y., Zhang, H., & Zhu, W.-G. (2013). Methylation of SUV39H1 by SET7/9 results in heterochromatin relaxation and genome instability. *Proceedings of the National Academy of Sciences*, *110*(14), 5516–5521. https://doi.org/10.1073/pnas.1216596110

Wong, P. G., Winter, S. L., Zaika, E., Cao, T. V., Oguz, U., Koomen, J. M., Hamlin, J. L., & Alexandrow, M. G. (2011). Cdc45 Limits Replicon Usage from a Low Density of preRCs in Mammalian Cells. *PLoS ONE*, *6*(3), e17533. https://doi.org/10.1371/journal.pone.0017533

Yeeles, J. T. P., Deegan, T. D., Janska, A., Early, A., & Diffley, J. F. X. (2015). Regulated eukaryotic DNA replication origin firing with purified proteins. *Nature*, *519*(7544), 431–435. https://doi.org/10.1038/nature14285

Yuan, K., & O'Farrell, P. H. (2016). TALE-light imaging reveals maternally guided, H3K9me2/3-independent emergence of functional heterochromatin in *Drosophila* embryos. *Genes & Development*, *30*(5), 579–593. https://doi.org/10.1101/gad.272237.115